PNAS

Supporting Information for the manuscript entitled:

The mRNA stability factor Khd4 defines a specific mRNA regulon for membrane trafficking in the pathogen *Ustilago maydis*

Srimeenakshi Sankaranarayanan[a], Carl Haag[a], Patrick Petzsch[b], Karl Köhrer[b], Anna Matuszyńska[c], Kathi Zarnack[d, e, 1] and Michael Feldbrügge[a, 1]

[1] co-corresponding authors

[a] Heinrich Heine University Düsseldorf, Institute for Microbiology, Cluster of Excellence on Plant Sciences, 40204 Düsseldorf, Germany.

[b] Biologisch-Medizinisches Forschungszentrum (BMFZ), Heinrich Heine University Düsseldorf, Universitätsstr. 1, 40204 Düsseldorf, Germany.

[c] Computational Life Science, Department of Biology, RWTH Aachen University, Worringerweg 1, 52074 Aachen, Germany.

[d] Buchmann Institute for Molecular Life Sciences (BMLS), Goethe University Frankfurt, 60438 Frankfurt a.M., Germany.

[e] Institute of Molecular Biosciences, Goethe University Frankfurt, 60438 Frankfurt a.M., Germany.

1   Supporting Information Text

Rrm4 is a key RBP for endosome-dependent RNA transport in *U. maydis*

In highly polarized cells such as fungal hyphae, the active trafficking of mRNA determines the spatial and temporal regulation of subcellular protein expression levels. A well-studied translocation mechanism is the endosome-dependent long-distance transport of mRNAs along microtubules in the dimorphic plant pathogen *Ustilago maydis*. The key transport unit of this machinery is Rrm4, one of the best-characterized RNA-binding proteins in fungal pathogens (1). Rrm4 contains three N-terminal RRM domains for RNA binding and three C-terminal MLLE domains for protein-protein interaction. Loss of Rrm4 abolishes mRNA transport, causing defective hyphae, with increased bipolar growth and reduced insertion of basal septa (Fig. S2C-D). A recent *in vivo* iCLIP study revealed that Rrm4 binds to a diverse set of mRNAs, accounting for over 60% of protein-coding genes in *U. maydis.* The binding study also revealed that the third RRM domain specifically recognizes the UAUG motif present in the mRNA targets (iCLIP- individual-nucleotide resolution cross-linking and immunoprecipitation; Fig. S4E; 2). This comprehensive knowledge of Rrm4 in terms of its RNA binding property provides an excellent model to validate the target identification capacity of hyperTRIBE in fungi.

Fusion of Ada preserves the function of Rrm4

To develop Rrm4-hyperTRIBE, we fused Ada-Gfp to the C-terminus of Rrm4 and expressed the fusion protein using the arabinose-inducible P$_{crg1}$ promoter in the ip^s locus of a strain carrying *rrm4* deletion (Fig. S2A-B). Inhibiting P$_{crg1}$ expression in this strain produces a typical *rrm4* deletion phenotype, characterized by bipolar hyphal growth with reduced insertion of basal septa. The strain expressing Rrm4-Gfp without Ada served as a control (Fig. S2A-D). As expected, Rrm4-Gfp expression fully rescued the *rrm4Δ* phenotype, leading to unipolar growing hyphae akin to wildtype cells (Fig. S2C-D). While a similar effect was observed for Rrm4-Ada-Gfp expression, we also detected a significant number of bipolar hyphae, possibly due to its lower expression levels as a result of Ada fusion (Fig. S2C-D; Fig. S3B) Nevertheless, the fluorescence microscopy analysis revealed that the Rrm4-Ada-Gfp fusion proteins mainly localized to bidirectionally shuttling endosomes at a velocity similar to the Rrm4-Gfp control, suggesting that the Rrm4-Ada-Gfp fusion protein is functional (Fig. S2E-F). Expression of the control-Ada did not affect the phenotype of hyphal cells (Fig. S2D; Fig. S3A-C). We confirmed the expression of full-length fusion proteins upon arabinose induction, and noticed higher expression levels for Rrm4-Gfp control, explaining the intense signal in transport endosomes (Fig. S2E; Fig. S3A-B). In summary, the full-length Rrm4-Ada-Gfp fusion protein was successfully expressed in *U. maydis,* and the Ada fusion protein complements the function of wildtype Rrm4.

Rrm4-Ada-Gfp identifies bona fide Rrm4 targets

Despite being expressed at lower levels than control-Ada, Rrm4-Ada-Gfp expression yielded approximately 4000 editing sites per replicate, which is twice as many as control-Ada editing events (Fig. 2C; Fig. S4A). This finding aligns with the broad target repertoire of Rrm4, suggesting that the magnitude of Ada editing is proportional to the binding landscape of the attached RBP. In addition to Ada editing frequency, the reproducibility of Ada editing was similar between Rrm4-Ada-Gfp and control-Ada, most likely due to the promiscuous and broad RNA binding tendencies of Rrm4 (Fig. S4B-D).

Comparing reproducible editing events from Rrm4-Ada-Gfp and control-Ada revealed 1124 and 649 unique editing events, respectively, with 480 editing sites shared between the two sets (Fig. 2C). Notably, 84% of mRNAs with unique Rrm4-Ada-Gfp editing events were bona fide Rrm4 iCLIP targets, while the enrichment of Rrm4 iCLIP targets in mRNAs with editing sites unique to control-Ada was lower (Fig. S4E-F; 73% of transcripts). Transcripts specific to overlapping editing events showed higher enrichment for Rrm4 iCLIP targets than control-Ada, suggesting Rrm4-Ada-Gfp specific editing (Fig. S4F; ~83% of transcripts).

Analyzing the spatial distribution of editing events relative to Rrm4 binding sites revealed that editing sites on mRNAs unique to Rrm4-Ada-Gfp were predominantly located in proximity to the actual Rrm4 binding site, with the number of editing events decreasing as the distance increased. (Fig. 2D, left panel; median distance=159 nt). Although there was significant enrichment for Rrm4 iCLIP targets, the editing sites in mRNAs specific to control-Ada were not enriched towards Rrm4 iCLIP binding sites (Fig. 2D, left panel; median distance=628 bp). Rrm4 contains three RNA Recognition Motifs (RRM3), and previous iCLIP experiments have shown that about one-third of Rrm4 binding sites encompass the UAUG motif that is bound by the third RRM domain (2). Notably, the editing sites on mRNAs specific to Rrm4-Ada-Gfp were also enriched in proximity to the UAUG-containing binding sites (Fig. 2D, right panel; median distance to nearest iCLIP site with UAUG motif: Rrm4-Ada-Gfp=252 nt, control-Ada=695 nt). These findings indicate that Ada editing is highly specific towards the true binding sites of the attached RBPs and distinct from background Ada editing. For instance, in target mRNA *ubi1,* encoding a natural fusion protein of ubiquitin and ribosomal 60S subunit protein L40 fusion protein, the editing site is found closer to the UAUG-containing binding site (3; Fig. S4G). Nonetheless, a *de novo* motif prediction around the Rrm4-Ada-Gfp editing sites using XSTREME did not yield a conclusive motif, possibly because the UAUG binding motif is only bound by the third RRM domain of Rrm4 and no other motif for the other two RRM domains could be identified to date (26). In summary, these results confirm that Ada editing events are guided by the attached RBP and hyperTRIBE can identify true RBP targets in fungal pathogens.

Mathematical modeling to study dynamic mRNA concentration changes

To test the effect of mRNA stability we have employed a well-established, single-compartment mathematical model of mRNA, as presented in the original work by

Hargrove and Schmidt (4) and White, Brewer and Wilson (5). mRNA concentrations can be modified by altering the rates of synthesis ($v_{\text{synthesis}}$) and/or degradation ($v_{\text{degradation}}$):

$$\frac{d[\text{mRNA}]}{dt} = v_{\text{synthesis}} - v_{\text{degradation}}$$

where mRNA synthesis is modeled with zero-order rate kinetics and rate of degradation with first-order kinetics.

$$v_{\text{synthesis}} = k_{\text{synthesis}}$$

$$v_{\text{degradation}} = k_{\text{decay}} \cdot [\text{mRNA}]$$

We assume that the rate of mRNA decay is inversely related to the mRNA half-life ($t_{1/2}$):

$$t_{1/2} = \frac{ln2}{k_{\text{decay}}}$$

hence the longer half-time translates to a slower rate of mRNA decay

$$k_{\text{decay}} = \frac{ln2}{t_{1/2}}$$

For numerical integration, we implemented the model in Python and performed a set of experiments *in silico* to test the effect of perturbing either of the rates. The code is openly available under https://github.com/AnnaMatuszynska/mRNAturnoverkinetics.

Change in *mob1* steady-state levels during hyphal morphogenesis

In this simulation, we have solved the initial value problem for *mob1* in wildtype and *khd4Δ* cells during the morphological transition from yeast to hyphae. The steady-state mRNA levels of *mob1* were quantified in Transcripts per million (TPM) using RNA-seq data from the yeast and hyphal transcriptome of both wildtype and *khd4Δ* cells. In our RNA-seq data, we observed ~10-fold induction in *mob1* expression during hyphal morphogenesis (Fig. S12B). In *khd4Δ* cells, the 10-fold increase persisted, but the expression levels were elevated in both yeast and hyphal stage (Fig. S12B). Based on these results, for the wildtype, the starting condition is set to 30 TPM corresponds to the steady-state level of mRNA in yeast. In the hyphal stage, the steady-state level reaches 300 TPM (Fig. S12B). To obtain mRNA half-lives, we have utilized the estimated half-life from *S. cerevisiae* (6). Assuming that the half-life of *mob1* is 8 minutes, we have fitted the rate constant for the synthesis to reach the 300 TPM in a steady state:

$$\frac{d[\text{mRNA}]}{dt} = v_{\text{synthesis}} - v_{\text{degradation}} = 0$$

$$v_{\text{synthesis}} = v_{\text{degradation}}$$

$$v_{\text{synthesis}} = \frac{ln2}{t_{1/2}}[mRNA_{steady}] = \frac{ln2}{8}[300]$$

and simulated the change in mRNA over time. In wildtype cells, the onset of hyphal morphogenesis led to a 10-fold increase in *mob1* level, quickly reaching a new steady state within 57 min of induction. The rate of synthesis has been set to zero after 3 hours of induction (180 min) and we observed exponential mRNA decay leading to the original steady-state level within 80 min (Fig. S12C). Similarly, a change in mRNA concentration in the *khd4Δ* mutant has been simulated, using 80 TPM as a steady-state level in the yeast stage, and 800 TPM as a steady-state level in the hyphal stage (Fig. S12B). Notably, stabilizing the *mob1* mRNA to a half-life of $t_{1/2}$=22 min is sufficient to reach the increased steady-state levels without changing the rate of synthesis (Fig. S12C). Moreover, the stabilized *mob1* in *khd4Δ* cells takes longer than 6 hours to reach its original steady-state level after the termination of mRNA synthesis (Fig. S12C).

We also utilized the simple model to study the impact of mRNA stability kinetics on the response time required for mRNAs to reach the steady-state level (Fig. S12A). The model has been parametrized to achieve a 10-fold increase for each mRNA type (Fig. S12A; unstable, moderately stable, and stable mRNAs), starting from an initial concentration of 1. The rate of synthesis was calibrated as earlier to reach a steady-state level that was 10-fold higher than the initial concentration. The half-lives of mRNAs were estimated from *S. cerevisiae* (6).

Our model revealed that the response times of mRNAs are based on their stability characteristics. Unstable mRNAs, characterized by a faster synthesis rate (0.87 transcript/min) and faster decay ($t_{1/2}$=8 min), exhibited a rapid response, reaching the steady state approximately in 1 hour after induction (Fig. S12A). In contrast, stable mRNA, with a slower synthesis rate (moderately stable mRNA=0.3 transcripts/min; stable mRNA=0.12 transcript/min) and slower decay (moderately stable mRNA, $t_{1/2}$=22 min; stable mRNA, $t_{1/2}$=60 min), required a longer time to reach the steady-state, indicating a delayed response (Fig. S12A). These findings highlight the importance of intrinsically unstable mRNA in achieving rapid on-off kinetics and facilitating faster cellular response.

Overall, our mathematical models emphasize the significant role of mRNA turnover kinetics in precisely controlling gene expression levels following transcriptional induction.

2   Materials and methods

Plasmids, strains, and growth conditions

For molecular cloning of plasmids, the *E. coli* K-12 derivative Top10 (Life Technologies, Carlsbad, CA, USA) was used. All *U. maydis* strains used in this study are derivatives of AB33 and generated by transforming the cells with linearized plasmids (7-9). For ectopic integration of hyperTRIBE constructs (Fig. 2B), the plasmids were linearized with AgeI (New England Biolabs) and integrated into the ip^s locus (10). For ectopic integration into the *upp3* locus, the plasmids were linearized using SwaI (NEB) restriction enzyme (11). Genomic DNA of wildtype strain UM521 (*a1b1*) was used as a template for PCR amplification. For RNA-editing, the amino acid sequence of the ADAR catalytic domain from *D. melanogaster* (Accession number: AHN59262.1; starting from M271 till E669) carrying the hyperactive E488Q mutation (12) was used (13, 14). The DNA sequence corresponding to the ADAR catalytic domain was codon-optimized for *U. maydis* before fusing to the RNA-binding protein of interest. Proteins were tagged with eGfp (enhanced green fluorescent protein; Clontech, Mountain View, CA, USA), or mKate2 (Kat; 15) for detection. All the plasmids were verified using Sanger sequencing. The homologous integration in *U. maydis* was validated by colony-PCR and Southern blot analysis. Detailed information about the strains, plasmids, and primers is given in Table S1-S4. The accession number of *Ustilago maydis* genes used in this study: *khd4* (UMAG_03837), *did2* (UMAG_05607), *rrm4* (UMAG_10836), *arl1* (UMAG_10313), *vma21* (UMAG_11418), *hok1* (UMAG_11790).

The conditions for *U. maydis* cultivation are described elsewhere (7). In short, yeast cells were grown in a complete medium (CM) medium supplemented with 1% glucose or 1% arabinose up to an OD_{600} of 0.5 at 28 °C on a rotary shaker at 200 rpm. To induce hyphal growth, yeast cells of 0.5 OD_{600} were shifted to nitrate minimal (NM) medium consisting of 1% glucose or 1% arabinose and grown for 6, 9, 10, and 12 hours (h.p.i.; hours post induction) at 28 °C. In addition to CM medium supplemented with arabinose (1%), the strains expressing arabinose-inducible Khd4 were also grown on CM medium supplemented with glucose (1%) in parallel to repress Khd4 expression, unless otherwise stated.

HyperTRIBE experiment and data processing

HyperTRIBE strains were grown consistently under arabinose-induced promoter-on conditions. Hyphae were induced by shifting 50 ml of exponentially growing cells from CM to NM medium, each supplemented with 1% arabinose. After 6 hours, the hyphal cells were harvested by centrifugation at 7546 *g* for 10 min at 4 °C. Cell pellets were resuspended in 1 ml ice-cold nuclease-free water and transferred to a 2 ml centrifuge tube. Cells were harvested at 7546 *g*, for 10 min at 4 °C, and the supernatant was removed completely. The resulting cell pellets were flash-frozen in liquid nitrogen and stored at -80 °C until further use.

Total RNA was extracted using the RNeasy Plant Mini Kit (74904; Qiagen, Hilden, Germany) following the manufacturer's instructions. Cell pellets were mechanically lysed at 30 Hz for 5 min at 4 °C in Mixer Mill MM400 (Retsch, Haan, Germany), in the presence of glass beads and Buffer RLC (+ß-mercaptoethanol). The resulting cell lysate was transferred to the QIAshredder spin column for further homogenization. The supernatant was transferred to a new centrifuge tube, mixed with 1 volume of 70% ethanol, and added to the RNeasy spin column. The subsequent steps were performed as per the manufacturer's protocol. To eliminate genomic DNA contamination, the on-column DNase digestion was performed using the RNase-Free DNase set (79254; Qiagen, Hilden, Germany). VAHTS® Universal V6 RNA-seq Library Prep Kit for Illumina (NR604-01/02; Vazyme) was used for cDNA library generation. All cDNA libraries expressing hyperTRIBE constructs sequenced using the HiSeq 3000 platform (Illumina), were processed simultaneously to obtain 151 nt single-end reads.

The bioinformatics analyses were based on the *U. maydis* 521 genome sequence (Ustilago_maydis.Umaydis521_2.0.dna_rm.chromosome) and the associated gene annotation (Ustilago_maydis.Umaydis521_2.0.41.gff3; both downloaded from http://ftp.ensemblgenomes.org/pub/fungi/release-53/fasta/ustilago_maydis/dna/; 16). To incorporate potential 5´ UTR and 3´ UTR regions, which are not currently annotated in the *Ustilago maydis* genome, we manually extended all genes by 300 nucleotides (nt) on each side. This extension was determined based on the transcript read coverage profile (Fig. S13E-F; see Differential gene expression analysis). While the majority of UTRs were shorter than 150 nt, we observed a subset of transcripts with UTRs spanning 300 nt in length. To ensure comprehensive coverage of all potential editing sites, we decided to manually extend the genes by 300 nt on both sides of the open reading frame (ORF). The extended GTF file was converted to refFlat format using the UCSC gtfToGenePred tool.

The A-to-G editing events on transcripts were identified using the wtRNA-RNA approach from the previously established hyperTRIBE pipeline (17; https://hypertribe.readthedocs.io/en/latest/run.html#b-find-rna-edit-sites-using-wtrna-rna-approaches). In brief, RNA-seq reads were trimmed based on sequencing quality (Phred score) using Trimmomatic (version 0.39; 18). Specifically, reads with a Phred score of less than 25 were trimmed and removed when the read length fell below 19 nt. The trimmed reads were then mapped to the *U. maydis* genome sequence and gene annotation using STAR (version 2.5.2b; 19), allowing reads that were mapped to exactly one location, had a minimum of 16 matched bases, and contained no more than 7% mismatches per mapped length. Uniquely mapped alignments in SAM format were loaded into a MySQL table with genomic coordinates. The nucleotides at each position in the test mRNA libraries (RBP-Ada-Gfp, control-Ada) were compared with those of the control mRNA library (wtRNA: RBP-Gfp) to identify A-to-G editing sites. Only editing events with a minimum of 20 read coverage and 5% editing were considered for further analysis. Editing sites that are assigned to more than one gene were removed from the analysis. From this, the list of reproducible editing sites that were consistently present in both replicates of either RBP-Ada-Gfp or control-Ada libraries was

identified. The resulting reproducible editing events from RBP-Ada-Gfp and control-Ada were compared against each other to determine the editing sites that were unique to RBP-Ada-Gfp (Fig. S4A, S6A).

Subcellular localization of proteins was defined using DeepLoc-2.0 (20; https://services.healthtech.dtu.dk/service.php?DeepLoc-2.0) and the cellular compartment ontology. Cellular compartment ontology annotations for *U. maydis* genes were downloaded from QuickGO (21, 22; https://www.ebi.ac.uk/QuickGO/annotations). A gene was assigned to more than one category if they were predicted to localize in more than one subcellular region.

De novo motif discovery

For *de novo* motif discovery, we first extracted sequences by extending 250 nt on both sides of the editing sites using Biostrings (R package; version 2.56.0). We employed XSTREME from the MEME suite for motif discovery and enrichment analysis (23). Sequences of length 501 nt were randomly selected from the *U. maydis* genome and used as a background control (random genome background). XSTREME analysis was conducted using default parameters. The relative enrichment ratio (tested sequences vs. random genome background) of the identified motifs was compared against the absolute percentage of tested sequences with enriched motifs. Only motifs that exhibited both high enrichment and overrepresentation were considered potential RBP binding motifs. Motif logos were created using the ggseqlogo package (version 0.1) in R, utilizing the position-specific weight matrix (PWM) of the identified motifs.

Motif analysis

The genomic position of the AUACCC, AGAUCU, GGGUAU, and ACACUC motifs on the *U. maydis* 521 genome sequences (PEDANT database name p3_t237631_Ust_maydi_v2GB) was identified using the Bioconductor package GenomicRanges in R (version 1.40.0; https://bioconductor.org/packages/release/bioc/html/GenomicRanges.html). Sequence information was extracted using Biostrings (R package; version 2.56.0; https://bioconductor.org/packages/release/bioc/html/Biostrings.html). To determine the genomic position of the *de novo* discovered motifs. The matchPWM function from the Biostrings R package was employed to perform the motif-matching process.

To calculate the distance between hyperTRIBE editing sites and the nearest motif, we first obtained the genomic coordinates of editing sites. We then proceeded to determine the distance of each editing site to the nearest motif using the nearest-methods function in the GenomicRanges R package.

To assess motif enrichment across transcript regions (Fig. 3F; Fig. S10A; Fig. S11A), we first determined the relative position of the motifs within the specific transcript regions, namely the 5´ UTR, ORF, and 3´ UTR. This was achieved by calculating the ratio between the distance from the motif start and the start codon to the length of the coding sequence (CDS). A ratio value ranging from 0 to 1 indicates a position within

the ORF, a negative value suggests motif occurrence in the 5´ UTR, and a value greater than 1 suggests motif incidence in the 3´ UTR. For regions on the "-" strand, we multiplied the resulting position by -1, to appropriately represent the motif positions on the antisense strand, ensuring that the relative positions remained comparable between the two strands. Motif enrichment analysis was then carried out by computing the relative proportion of motifs within different transcript regions.

For relative motif position calculation in SI Appendix, Fig. S8D, we first selected a window of 1000 nt with a start or stop codon at the center. We then obtained the genomic coordinates of the AUACCC and AGAUCU motifs within the selected window. The relative position of the motif on target transcripts was calculated by measuring the distance between the motif start position and the start or stop codon.

Differential gene expression analysis

Total RNA from yeast and hyphal (9 h.p.i.) cells was extracted using RNeasy Plant Mini Kit (74904; Qiagen, Hilden, Germany) following the manufacturer's protocol (see HyperTRIBE experiment and data processing). cDNA libraries were prepared using VAHTS® Universal V6 RNA-seq Library Prep Kit for Illumina (NR604-01/02; Vazyme) and sequenced using the HiSeq 3000 platform (Illumina), to obtain 151-nt single-end reads. Approximately, ~10 million raw reads for hyphal and ~20 million raw reads for yeast samples were obtained.

Basic quality control checks on all sequencing datasets were performed using FastQC (https://www.bioinformatics.babraham.ac.uk/projects/fastqc/). RNAseq data analysis was carried out in Galaxy, an open-source platform (24). The raw sequencing reads were quality filtered based on their quality score and length with Trimmomatic (Version 0.36; 18). Specifically, the reads were trimmed 20 nt from the start, trimmed from the end when the Phred score dropped below 30, and discarded if the read length is less than 20 nt. STAR (version 2.7.2b) was used to align the trimmed reads to the *U. maydis* genome (see HyperTRIBE experiment and data processing; 19), allowing up to 4% mismatches in the mapped read length while limiting the mapping to one locus. Uniquely mapped reads on each gene were counted using htseq-count (version 0.9.1; 25). The resulting raw counts of mRNA libraries were used as input for the subsequent differential gene expression analysis. All differential gene expression analysis was performed using the R/Bioconductor package DESeq2 (26). Genes with an absolute fold change>1.5 (after fold change shrinkage) and an adjusted P<0.05 (Benjamini-Hochberg correction) were considered differentially expressed.

To identify differentially expressed genes in hyphae following a morphological switch from yeast, quantitative changes in transcript expression levels were calculated by comparing the hyphal against the yeast mRNA libraries ("hyphae vs. yeast") for wildtype as well as *khd4Δ* strains. As a result, transcripts that were more expressed in the hyphal form obtained a positive $\log_2$-transformed fold change ($\log_2$ fold change), while transcripts that were more expressed in the yeast form obtained a negative $\log_2$ fold change. To identify differentially expressed genes in the hyphal cells after *khd4*

deletion, the mRNA libraries from the *khd4Δ* hyphal cells (9 h.p.i.) were compared against the mRNA libraries of wildtype hyphal cells (9 h.p.i.) ("*khd4Δ* hyphae vs. wildtype hyphae").

To identify potential UTR regions, the transcript read coverage profile was generated by analyzing the mapped BAM files (Fig. S13A). The coverage function from the IRanges package (R package version 2.32.0) was utilized to calculate the coverage of the mapped BAM file. Subsequently, each coverage value was normalized by dividing it by the total number of reads. To focus on regions surrounding the start or stop codons, we extracted the coverage values within a 501 nt window centered around these codons. These extracted values were then converted to z-scores by subtracting the mean of the respective row from each element in that row and dividing the result by the standard deviation of the row.

Gene ontology (GO) term enrichment analysis

Functional enrichment analysis was performed in R using the R package gprofiler2 (e107_eg54_p17_bf42210; version 0.2.1; https://cran.r-project.org/web/packages/gprofiler2/vignettes/gprofiler2.html; 27, 28). For the g:Gost analysis, multiple testing correction was performed with the default g:SCS method and a p-value threshold of 0.05. Downloaded Generic EnrichmentMap (GEM) file from g:Profiler was loaded into the Cytoscape (version 3.8.0) plugin, EnrichmentMap (version 1.1.0) to visualize the GO term enrichment analysis (Jaccard coefficient cutoff of >0.25). The clusters were identified and annotated according to the GO-term annotation of the gene sets using the Cytoscape plugins AutoAnnotate (version 1.3.5) and the WorldCloud app (version 3.1.4) (29-31).

Reporter fluorescence measurement

Hyphal growth was induced by shifting 20 ml of exponentially growing yeast cells in CM medium to NM medium, each supplemented with 1% glucose (promoter-off condition) or 1% arabinose (promoter-on condition). After 6 hours 1 ml of culture was harvested at 16000 *g* for 5 min at room temperature. Cell pellets were washed twice in double-distilled water. After harvesting, the supernatant was removed completely. The resulting cell pellets were resuspended using 1 ml of double-distilled water. 200 µl of samples were transferred into black 96-well plates (Greiner 96 Flat Bottom Black Polystyrene: Greiner, Frickenhausen, Germany). Optical density (OD_{600}) and mKate2 fluorescence level (excitation wavelength: 588 nm, emission wavelength: 633 nm) were measured in an Infinite M200 plate reader (Tecan Group Ltd., Männedorf, Switzerland). The fluorescence levels (mKate2) were normalized to the optical density of the cell culture (OD_{600}). The strain constitutively expressing mKate2 (*kat_no motif*) was used for calculating relative mKate2 protein abundance (Table S1). Statistical significance was calculated using multiple Student's *t*-test in Prism version 5.04 (GraphPad, La Jolla, CA, USA).

RT-qPCR analysis

Total RNA from hyphal cells (6 h.p.i.) was extracted using the RNeasy Plant Mini Kit (74904; Qiagen, Hilden, Germany) as described earlier (see HyperTRIBE experiment and data processing). 1 µg of total RNA served as a template for first-strand cDNA synthesis with oligo (dT) primers using ProtoScript® II First Strand cDNA Synthesis Kit (NEB). 1 µl of cDNA was used per reaction in qPCR, following the standard Luna® Universal qPCR Master Mix (NEB) protocol in Stratagene Mx3000P (Agilent Technologies). Relative gene expression value was calculated as $\exp(-\Delta C_t)$ (threshold cycles) ratios, with UMAG_04871 (phosphoglycerate kinase; $\log_2$-transformed fold change=0.1, adjusted P=0.55, in "*khd4Δ* hyphae vs. wildtype hyphae" RNA-seq analysis) as a reference gene. The abundance of *mkate2* mRNA was calculated relative to *mkate2* expression in the strain *kat_no motif*. Primers used for RT-qPCR are shown in Table S4. Statistical significance was calculated using multiple Student's *t*-test in Prism version 5.04 (GraphPad, La Jolla, CA, USA).

Ustilago maydis **cell disruption and immunoblotting analysis**

U. maydis cell disruption was performed as previously reported (32). In short, 50 ml of hyphal cells (6 h.p.i.; see Plasmids, strains, and growth conditions) were harvested by centrifugation at 7546 *g*, for 10 min. After washing in phosphate-buffered saline of pH 7.0, the samples were flash-frozen in liquid nitrogen and stored at -80 °C until further use. Samples were lysed using a 5 mm stainless-steel bead in Mixer Mill MM400 (Retsch, Haan, Germany) at 30 Hz for 1 min. Cell disruption was repeated 3 times with intermittent liquid cooling steps of 5 min. The resulting homogenized cell powder was resuspended in 1 ml urea buffer (8 M urea; 50 mM Tris/HCl pH 8; containing 1 mM DTT, 0.1 M PMSF, 1 tablet of cOmplete protease inhibitor per 25 ml, Roche, Mannheim, Germany) and centrifuged at 16,000 *g* for 10 min at 4 °C. The supernatant was used for subsequent analysis. Protein concentrations were measured with the Bradford assay (BioRad, Munich, Germany) as per the manufacturer's protocol. Sample volumes were adjusted to equal concentrations, supplemented with Laemmli buffer, and boiled at 95 °C for 10 min. Samples were resolved in 1.5 mm thick 8% SDS-PAGE and transferred to a nitrocellulose membrane (Amersham Protran) for immobilization by semi-dry blotting.

Proteins were detected using the primary antibodies, α-Gfp (Roche, Germany) and α-Actin from mouse (MP Biomedicals, Germany). α-mouse IgG HRP conjugate (Promega, Madison, WI, United States) was used as a secondary antibody. Antibodies bound to nitrocellulose membrane were removed by treating the blot in TBS buffer pH 3.0 (50 mM Tris pH 3.0, 150 mM NaCl) at room temperature, before detecting the constitutively expressed actin control. Detection was carried out using ECL™ Prime (Cytiva RPN2236;). Images were recorded by a luminescence image analyzer, LAS4000 (GE Healthcare).

Staining techniques

To visualize basal septa and empty sections, 1 ml of cell culture was stained with 1 µl of Calcofluor white staining solution (2 mg/ml; CFW) directly before microscopy with a DAPI filter set (33).

FM4-64 uptake assay was carried out as described previously (34). Hyphal growth was induced in NM medium for 10 hours. 1 ml of culture was transferred into a 2 ml centrifuge tube and incubated for 10 min on ice. 4 µM (final concentration) of FM4-64 was added to the cells and incubated for an additional 10 min on ice, protected from light. Cells were washed by centrifugation at 2400 g for 3 min at 4 °C. Cell pellets were resuspended in 1 ml of ice-cold NM-glucose medium. Samples were shifted to a thermoblock set at 1100 rpm and 28 °C for 25 min prior to visualization under fluorescence microscopy.

Vacuolar staining was performed using CMAC (7-amino-4-chloromethylcoumarin; ThermoFisher, Darmstadt, Germany). 1 ml of cell suspension was stained with 10 µM CMAC and incubated for 30 min at 28 °C on a rotating wheel. Cells were washed by centrifugation at 2400 g for 3 min. Subsequently, the cell pellets were resuspended in phosphate-buffered saline prior to microscopy with the DAPI filter set.

Microscopy and image processing

For microscopic analysis, 20 ml of yeast cells were grown in CM medium (1% glucose) to an OD_{600} of 0.5. Hyphal cells were induced by shifting 20 ml cell culture from CM medium to NM medium (supplemented either with 1% glucose or 1% arabinose) for 6, 9, 10, and 12 hours. All images and videos were acquired using laser-based epifluorescence-microscopy, Zeiss Axio Observer.Z1 (Oberkochen, Germany) as described previously (35). The exceptions are the images and videos requiring a filter set for DAPI (4′,6-diamidino-2-phenylindole) which was carried out by Zeiss Axio Imager M1 (Oberkochen, Germany) as indicated before (33). All movies and images were processed using the MetaMorph software package (version 7.7.0.0, Molecular Devices, Seattle, IL, USA).

The hyphal length was determined by measuring the distance between the tip and the basal pole without including the empty sections. Hyphal width was calculated by taking the average thickness measured at three different locations within each hypha. Hyphal cells with empty sections were visualized using Calcofluor White (CFW) and were scored manually. For each experiment, more than 100 cells were counted per strain.

To assess the FM4-64 (ThermoFisher) signal in hyphal cells, movies with an exposure time of 150 ms, and 100 frames were recorded. Kymographs from the movies were generated using the MetaMorph software package. Changes in direction were counted as an individual signal with the following parameters: a signal is processive if particles exhibit a directional travel distance of greater than 5 µm; diffusive if the signal traveled is less than 5 µm but greater than 0 µm. The diffusive particles display random

erratic movements without a clear trajectory. More than 25 hyphal cells were analyzed per strain (n=3 independent experiments).

Vacuole distribution was scored by acquiring z-stacks (z-distance- 0.23 µm) and analyzing the maximum projection. The intensity profile of CMAC-stained hyphal cells was performed by line scan. Fluorescent intensity was plotted against their respective position after subtracting the background fluorescence of the micrograph. Vacuole distribution and aberrant cortical localization were scored by visual inspection (Fig. 7A-D). For the quantification of vacuole distribution, the line scans (see above; Fig. 7A, bottom panel) were used to distinguish normal and disrupted distribution. The cortical localization of vacuoles at the cell edge was quantified by visually counting the cells exhibiting this phenotype. For each strain, more than 25 cells were analyzed.

All quantifications were performed using data obtained from three independent experiments. Data points represent the mean of independent experiments. Prism5 (GraphPad, La Jolla, CA, USA) was used for statistical analysis.

Multiple sequence alignments

Ortholog proteins were identified using BLASTP (https://blast.ncbi.nlm.nih.gov/Blast.cgi?PAGE=Proteins) and FungiDB (https://fungidb.org/fungidb/app). Multiple sequence alignment was carried out using Clustal Omega (36). Genedoc (version 2.6.002) was used for graphical representation.
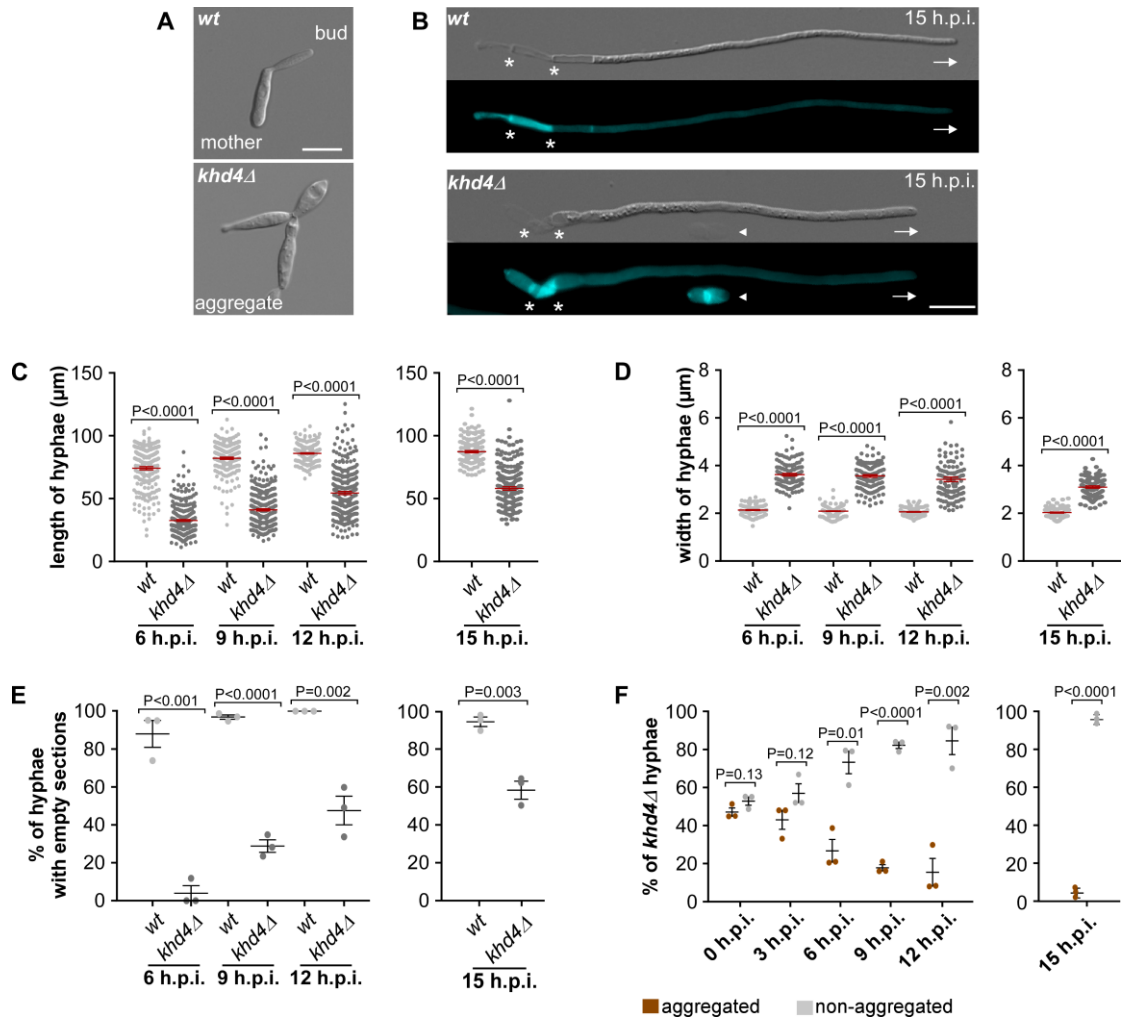
3   Supporting information Figures

Fig. S1. Loss of Khd4 affects the morphology of yeast as well as hyphal cells

(A) Differential interference contrast (DIC) images of yeast cells. **(B)** DIC (top panel) and calcofluor white-stained (CFW; bottom panel) images of hyphae grown for 15 h.p.i. (basal septum and growth directions are marked by asterisks and arrows, respectively; triangle indicates a broken empty section; scale bar: 10 µm). **(C)** Hyphal length over time. Data from n=3 independent experiments (>100 hyphae were counted per strain) are overlaid with the mean of means and standard error of the mean (s.e.m., red line). Statistical evaluation was performed using an unpaired two-tailed Student's *t*-test on mean length. **(D)** Hyphal width over time. (Shown are merged data from n=3 independent experiments; >100 hyphae were analyzed; error bars: s.e.m.; unpaired two-tailed Student's *t*-test on mean width). **(E)** Percentage of hyphae with empty sections over time. (Data points represent the average percentage from n=3 independent experiments; >100 hyphae were analyzed per strain; error bars: s.e.m.; unpaired two-tailed Student's *t*-test on the means). **(F)** Percentage of *khd4Δ* hyphae aggregated (brown) or non-aggregated (grey) at different time points. (Data points represent the mean hyphal percentage from n=3 independent experiments; >100 hyphae were counted per strain; error bars: s.e.m.; unpaired two-tailed Student's *t*-test on the means).
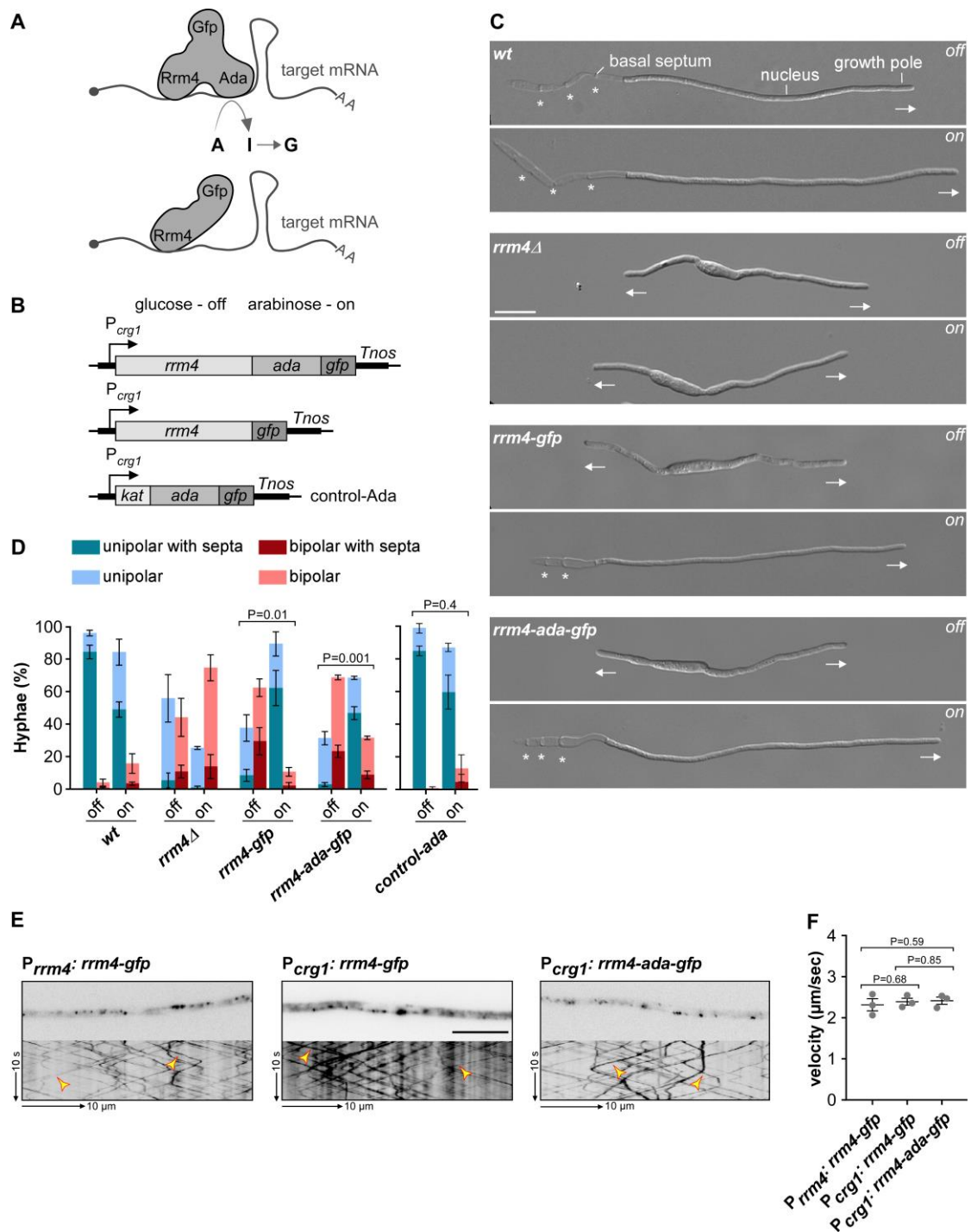
15

Fig. S2. Rrm4-Ada-Gfp fusion protein rescues *rrm4Δ* phenotype

(A) Top: Schematic representation of target RNA editing by hyperTRIBE. As the Rrm4-Ada-Gfp fusion protein binds to the target mRNA through Rrm4 (light blue), the fused Ada (dark blue) deaminates the adjacent adenosine (A) to inosine (I) which is converted to guanine (G). Bottom: The binding of control protein Rrm4-Gfp to the target mRNA (Ada- hyperactive version of *Drosophila* ADAR catalytic domain; Gfp- Green fluorescent protein; Filled circle- 5´cap structure; AA- poly(A) tail of target mRNA (grey). **(B)** Schematic representation of hyperTRIBE constructs with arabinose inducible P*crg1* promoter (on), which is repressed by glucose (off) (*Tnos*- transcription terminator). Fusion proteins of Rrm4, Ada, Gfp, and/or Kat (mKate2- red fluorescent protein; *Tnos*- transcription terminator). The hyperTRIBE constructs

are expressed in a strain carrying *rrm4Δ* genetic background. **(C)** DIC images of AB33 hyphal derivatives (6 h.p.i.) under promoter uninduced off (top) and promoter induced on (bottom) conditions. (Arrows and asterisks indicate growth direction and empty sections, respectively; scale bar- 10 µm). **(D)** Quantifying the growth of AB33-derived hyphal cells shown in B (6 h.p.i.). Unipolarity, bipolarity, and basal septum formations were quantified (error bars: s.e.m.; >100 hyphal cells from n=3 independent experiments were quantified per strain; unpaired two-tailed Student's *t*-test was used for the statistical evaluation of the percentage unipolarity and bipolarity). **(E)** Inverted fluorescent images (top) and their corresponding kymographs (bottom) of AB33-derived hyphal cells (6 h.p.i.) expressing green fluorescent proteins under promoter on condition. P$_{rrm4}$: *rrm4-gfp* refers to the strain where Rrm4-Gfp is expressed under the endogenous condition. Example processive moving signals are indicated by yellow arrowheads. **(F)** The average velocity of fluorescent signals per 20 µm of hyphal length in AB33 hyphal derivatives is shown in D. For quantification, only processively moving particles (>5 µm) were considered. P$_{rrm4}$: *rrm4-gfp* refers to the strain where Rrm4-Gfp is expressed under the endogenous condition. Data points represent average velocities from n=3 independent experiments, with mean of means and s.e.m.; >25 hyphal cells were analyzed per strain; unpaired two-tailed Student's *t*-test.
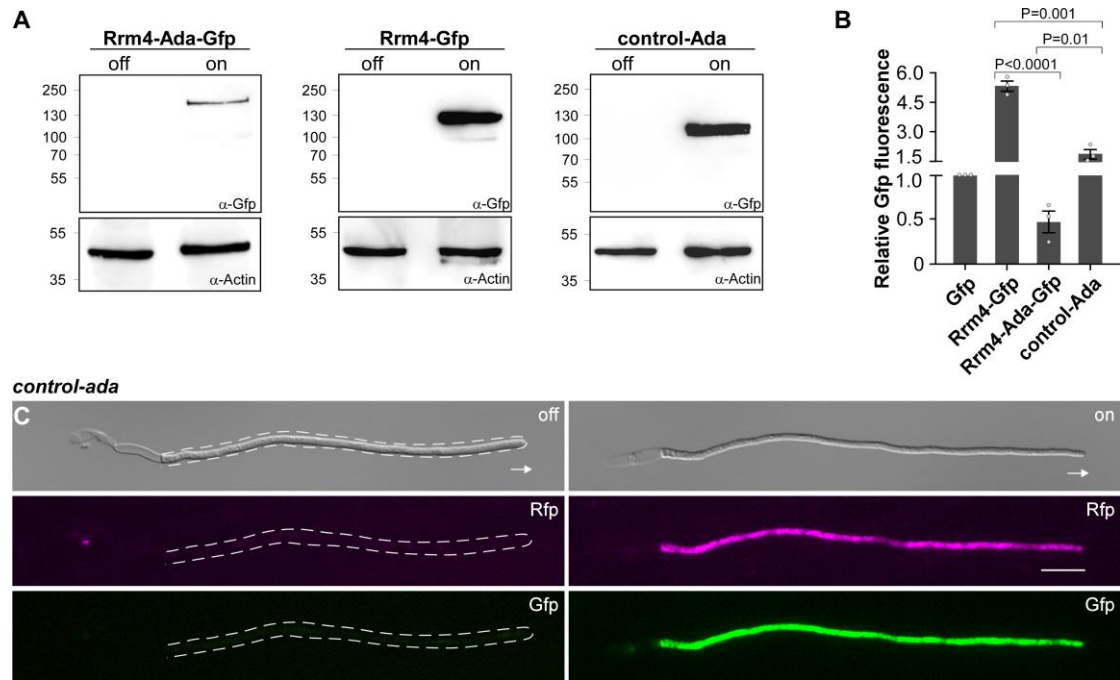
Fig. S3. Protein expression analysis of the Rrm4-hyperTRIBE constructs.

(A) Western blot analysis of the full-length fusion protein expression under promoter uninduced (off) and induced (on) conditions. Immunoblotting was performed using α-Gfp and α-Actin. The size of protein markers (kDa) is shown on the left. (Molecular weight of the full-length fusion proteins: Rrm4-Ada-Gfp- ~158 kDa; Rrm4-Gfp- ~112 kDa; control-Ada- ~99 kDa; Molecular weight of the individual proteins: Rrm4- ~85 kDa, Ada- ~44 kDa, Gfp- ~27 kDa, Kat- ~26 kDa). **(B)** Expression levels of Rrm4-hyperTRIBE constructs. Gfp fluorescence levels were calculated relative to the Gfp control. Statistical analysis was performed using the unpaired two-tailed Student's *t*-test on mean fluorescence level (n=3 independent experiments; error bars: s.e.m.). **(C)** DIC (top panel) and fluorescent images (Rfp- middle panels; Gfp- bottom panels) of hyphae (6 h.p.i.) expressing control-Ada under promoter uninduced off condition (left) and promoter induced on condition (right) (arrows indicate growth direction; scale bar: 10 μm).
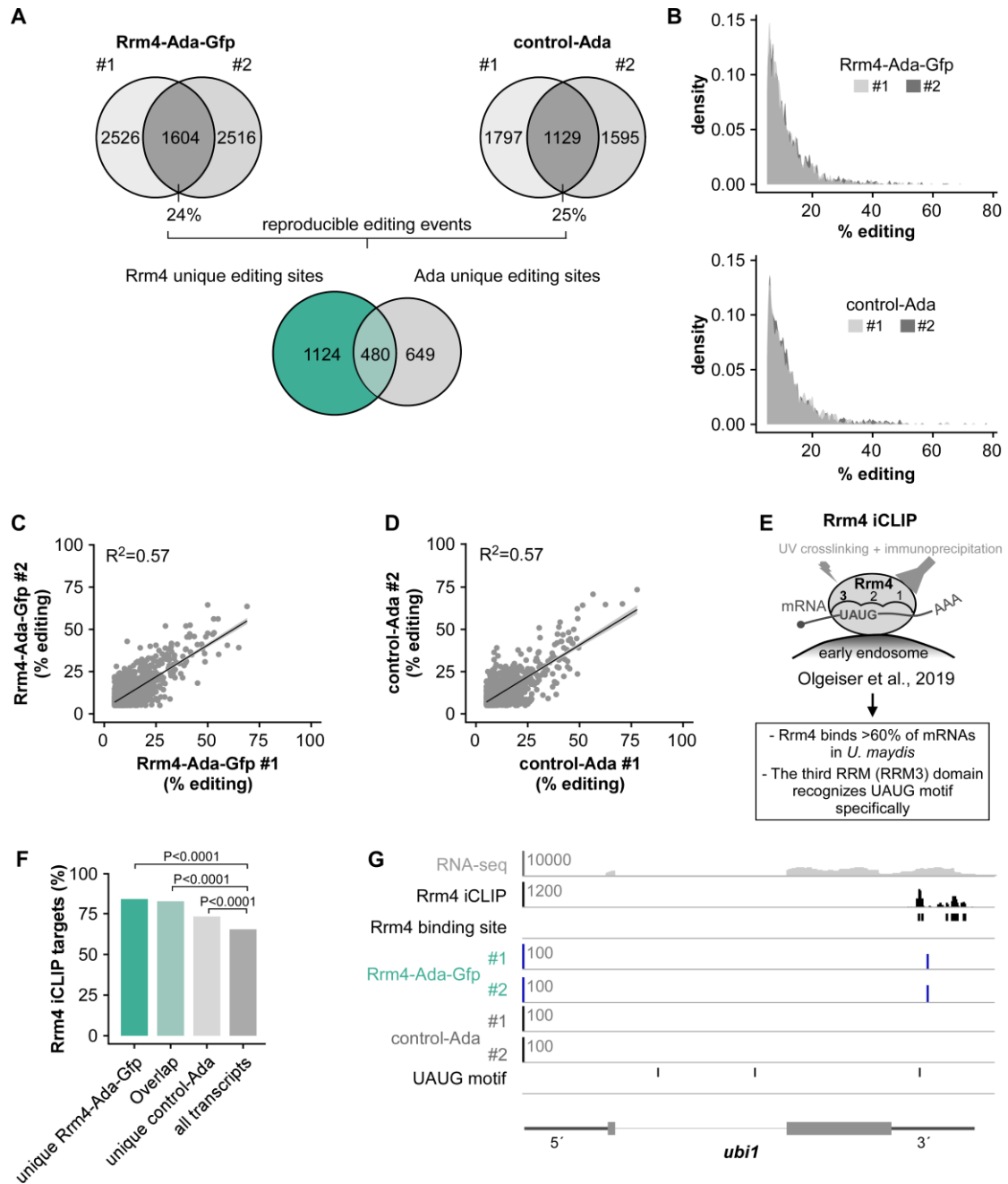
Fig. S4. Rrm4-Ada-Gfp identifies bona fide Rrm4 target mRNAs

(A) Overview of the hyperTRIBE workflow. Editing events overlapped between the two independent biological replicates of Rrm4-Ada-Gfp (sea green) and control-Ada (grey) data. The indicated values represent the number of editing events in each category. For the analysis, only editing events with ≥5% editing was considered (#1,2- replicates 1 and 2, respectively). Reproducible editing sites overlapped between the two independent biological replicates of the Rrm4-Ada-Gfp (blue) and control-Ada (grey) data were compared with each other. **(B)** Density plot comparing percentage editing in Rrm4-Ada-Gfp (top) and control-Ada (bottom). **(C, D)** Correlation of editing levels between two biological replicates of Rrm4-Ada-Gfp (C) and control-Ada (D) (R^2- coefficient of determination). **(E)** Schematic illustrating the iCLIP results of Rrm4, a key RBP involved in endosomal mRNA transport. The iCLIP method was employed to map the precise binding sites of Rrm4 across transcriptome (2). Rrm4 is a broadly binding RBP that interacts with more than 60% of mRNAs in *U. maydis*. The RRM3 domain recognizes

the UAUG motif on mRNA. **(F)** HyperTRIBE data of Rrm4 on the target transcript *ubi1* (UMAG_02440). Genome viewer tracks displaying RNA-seq read coverage (top panel; grey) followed by Rrm4 iCLIP crosslink signal (black) and the corresponding Rrm4 binding sites (black) as well as hyperTRIBE signal with editing events from Rrm4-Ada-Gfp (#1-replicate 1, #2-replicate 2; blue) and control-Ada. The position of the UAUG motif is indicated in the bottom track (black). Gene model with exon/intron structures below were extended by 300 nucleotides on either side to include 5´UTR and 3´UTR regions (grey). **(G)** Percentage of Rrm4 iCLIP targets in different transcript sets as indicated in D. Statistical significance was calculated using Fisher's exact test.
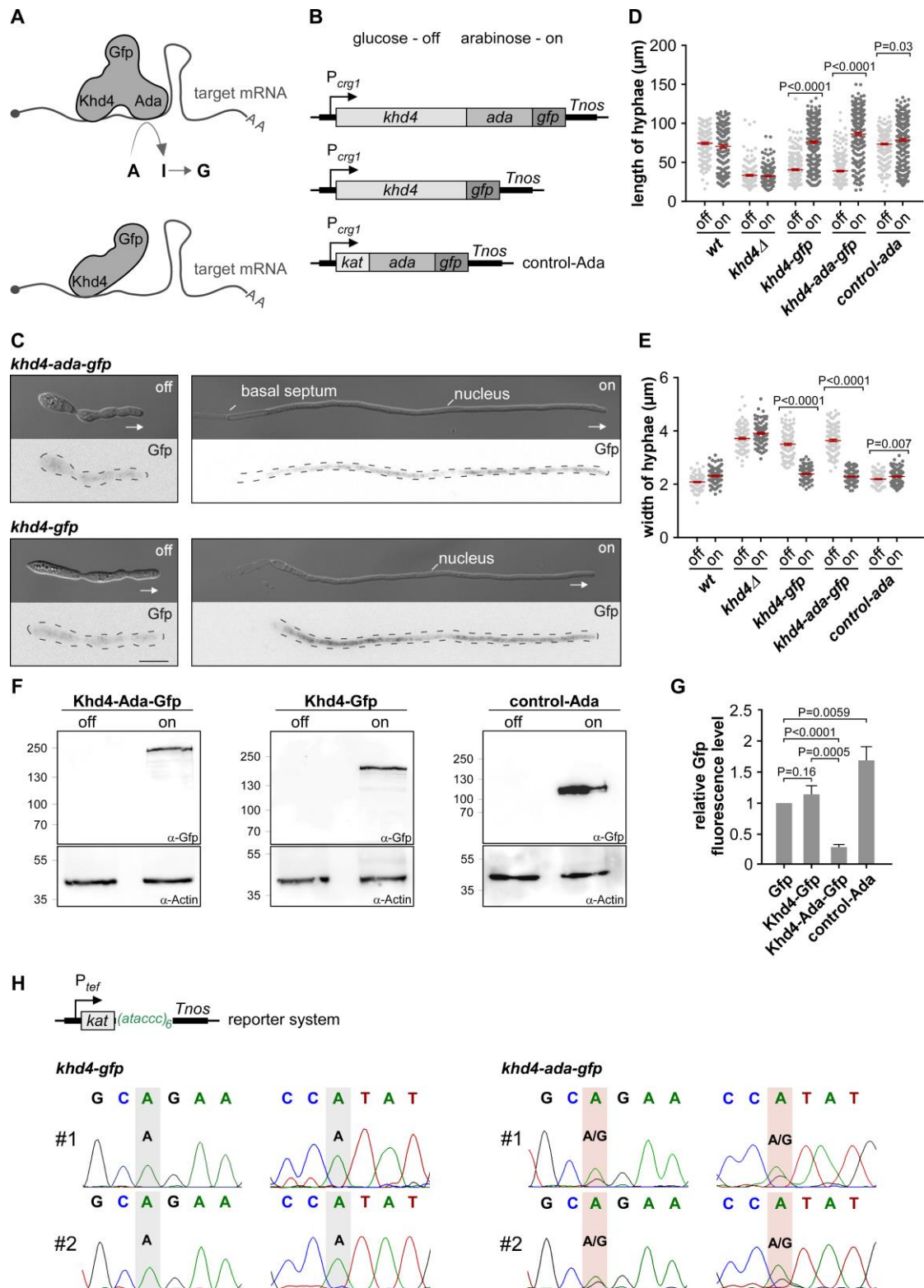
Fig. S5. Establishing hyperTRIBE to identify *in vivo* targets of Khd4

(A) Schematic illustration of the hyperTRIBE technique. The binding of Khd4-Ada-Gfp fusion protein to target mRNA results in the editing of adjacent adenosine (A) to inosine (I) which is converted to guanine (G; top). The interaction of control protein Khd4-Gfp to the target mRNA is given below (Ada- hyperactive version of *Drosophila* ADAR catalytic domain; Gfp- green fluorescent protein; AA- poly(A) tail, 5´ cap structure is depicted by a grey circle). **(B)**

Schematic representation of hyperTRIBE constructs with arabinose inducible P_{crg1} promoter (on), which is repressed by glucose (off). Fusion proteins of Khd4, Ada, Gfp, and/or Kat (mKate2- red fluorescent protein; *Tnos*- transcription terminator). The hyperTRIBE constructs are expressed in a strain carrying *khd4Δ* genetic background. **(C)** DIC (top panel) and fluorescent images (Gfp; bottom panel) of hyphae (6 h.p.i.) expressing hyperTRIBE constructs in the genetic background of the *khd4Δ* strain under promoter-uninduced off condition (left) and promoter-induced on condition (right) (arrows indicate growth direction; scale bar: 10 μm). **(D)** Length of hyphae: merged data from n=3 independent experiments (error bars: s.e.m. (red line); >100 hyphal cells per strain). Statistical analysis was conducted using the unpaired two-tailed Student's *t*-test on mean length. **(E)** Width of hyphae: merged data from n=3 independent experiments (error bars: s.e.m. (red line); >100 hyphae per strain were measured at three distinct positions within each hypha). Statistical analysis was performed using the unpaired two-tailed Student's *t*-test on mean width. **(F)** Western blot analysis of fusion proteins under uninduced (off) and induced (on) conditions. Results were analyzed with α-Gfp and α-Actin immunoblotting. The size of protein markers (kDa) is shown on the left. (Molecular weight of the full-length fusion proteins: Khd4-Ada-Gfp- ~224 kDa; Khd4-Gfp- ~179 kDa; control-Ada- ~99 kDa; Molecular weight of the individual proteins: Khd4- ~151 kDa, Ada- ~44 kDa, Gfp- ~27 kDa, Kat- ~26 kDa). **(G)** Expression levels of Ada-fusion protein under promoter-induced on condition. The Gfp fluorescence level was calculated relative to the Gfp control. Statistical analysis was performed using the unpaired two-tailed Student's t-test on mean fluorescence level (n=3 independent experiments; error bars: s.e.m.). **(H)** Upper part: reporter constructs expressing synthetic mRNAs containing *kat* coding sequence with the Khd4 binding element AUACCC (*(ataccc)₆;* green) in its 3´ UTR, driven by a constitutively active P_{tef} promoter. Lower part: Sanger sequencing of synthetic target mRNA isolated from strains expressing control Khd4-Gfp (left panel) and Khd4-Ada-Gfp (right panel). Data shown here are from two independent experiments (#1 and #2). Edited adenosines are highlighted. Double peaks corresponding to A and G are observed at the edited site.
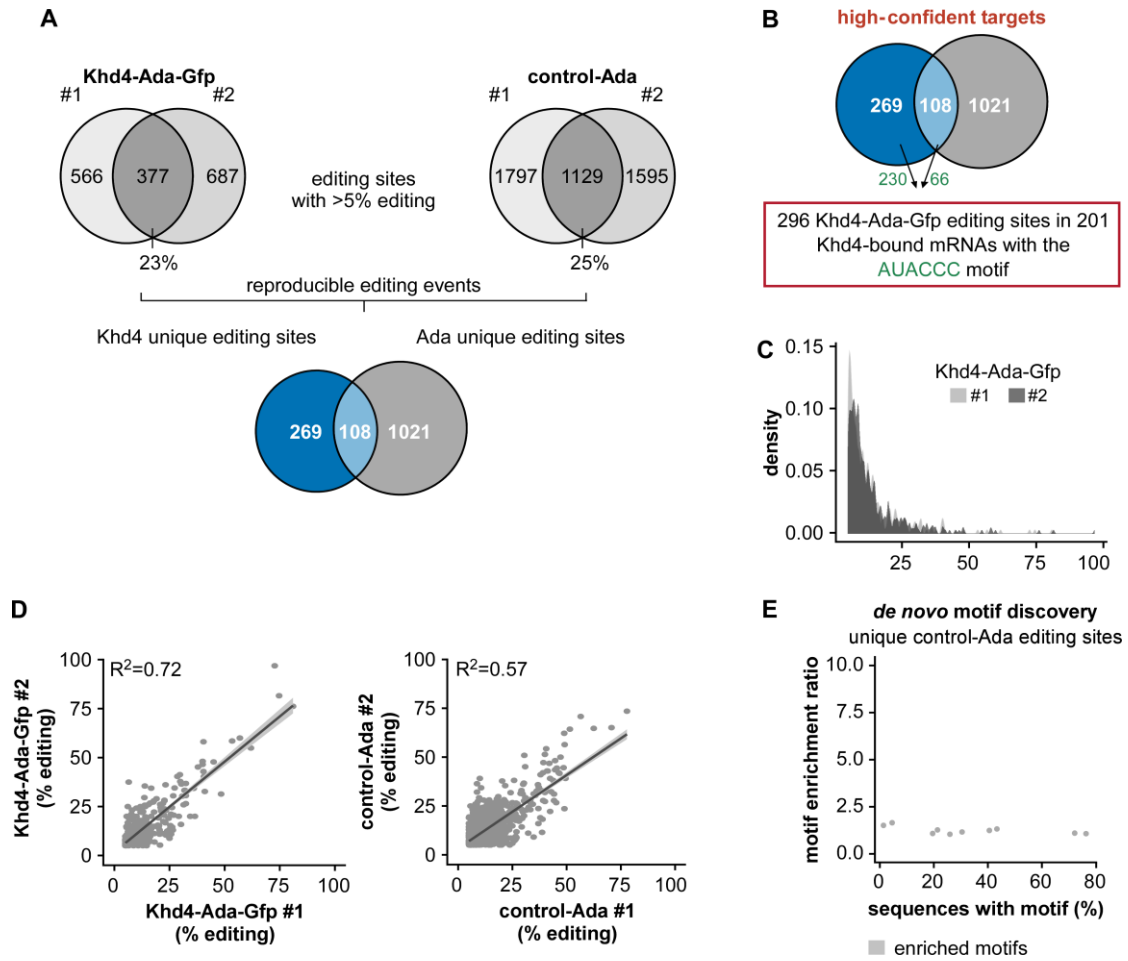
Fig. S6. Khd4-Ada-Gfp editing sites are highly reproducible.

(A) Overview of the hyperTRIBE workflow. Reproducible editing sites overlapped between the two independent biological replicates of the Khd4-Ada-Gfp (blue) and control-Ada (grey) data were compared with each other (#1,2- replicates 1 and 2). Only editing events with 5% editing were used for the analysis. **(B)** The genes corresponding to the Khd4-Ada-Gfp-specific editing sites (blue) were subsequently analyzed for the presence of the AUACCC binding motif and were defined as high-confident Khd4-bound mRNAs (red). High-confident editing sites from each respective category are indicated in green. **(C)** Density plot of percentage editing events in Khd4-Ada-Gfp. **(D)** Scatter plots comparing the correlation of editing levels between two replicates (rep#1,2- replicate 1 and 2) of Khd4-Ada-Gfp and control-Ada. (R^2- coefficient of determination). **(E)** *De novo* motif discovery analysis on sequences carrying unique control-Ada editing sites. Scatter plot comparing the enrichment ratio relative to the background (grey; random genome background) with the percentage of tested sequences containing the enriched motifs.
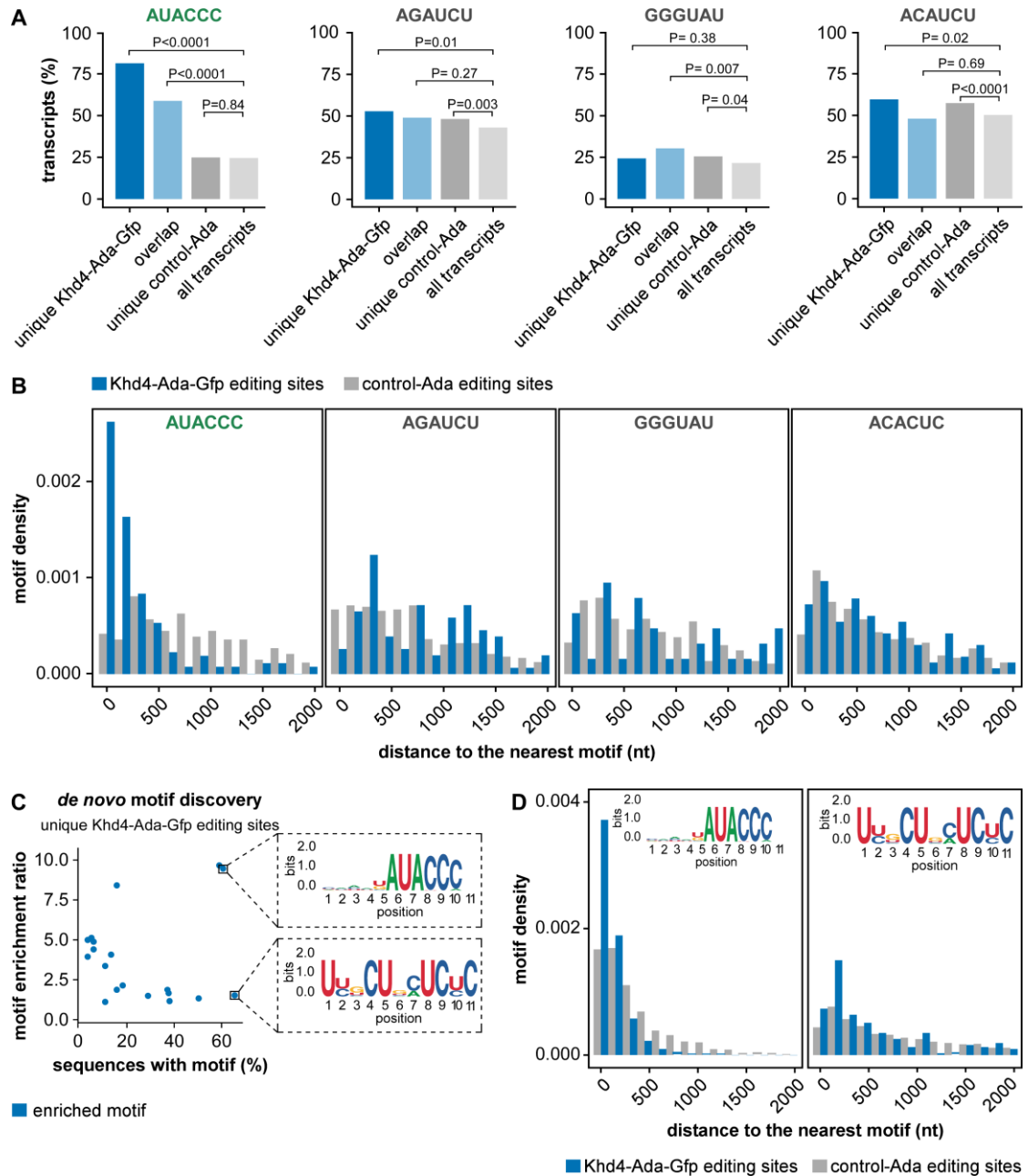
Fig. S7. Khd4-Ada-Gfp editing sites are proximal to the AUACCC motif

(**A**) Percentage of transcripts containing the AUACCC, AGAUCU, GGGUAU (antisense motif), and ACAUCU (scrambled sequence) motifs in different transcript sets as indicated in Fig. 3B. Statistical significance was determined using Fisher's exact test. (**B**) Histogram illustrating the distribution of editing sites from the nearest AUACCC, AGAUCU, GGGUAU, or ACACUC motifs in transcripts specific to Khd4-Ada-Gfp (blue) compared to control-Ada (grey). (**C**) Scatter plots comparing the relative enrichment ratio (tested sequence vs. random genome background) against the percentage of tested sequences carrying the enriched motifs (blue). Enlarged regions highlight the sequence logo of the selected motifs. Top: motif with a high enrichment ratio and overrepresentation. Bottom: highly overrepresented motif. (**D**) Histogram displaying the distribution of editing sites from the selected *de novo* discovered motifs in transcripts specific to Khd4-Ada-Gfp (blue) and control-Ada (grey). The corresponding sequence logos of the motifs are displayed inside.
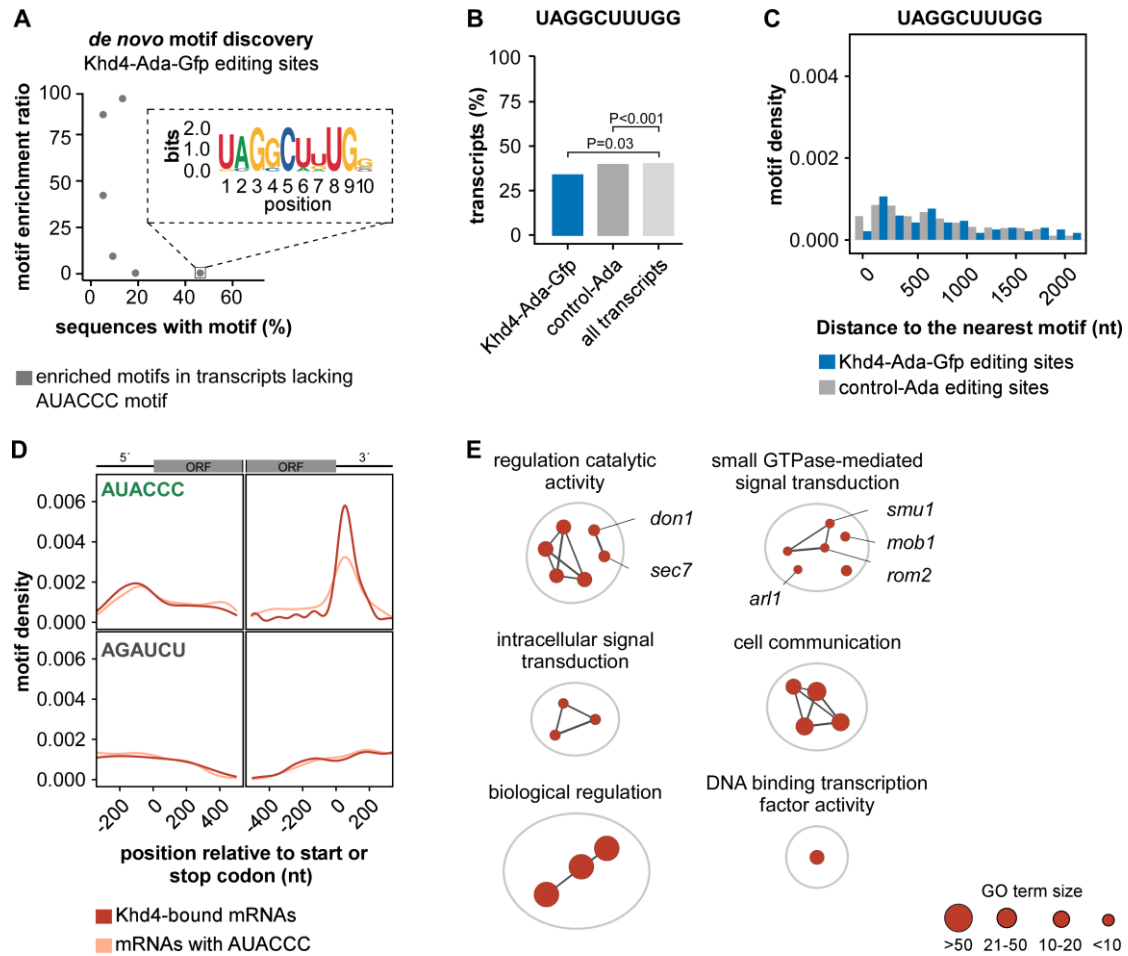
24

Fig. S8. Khd4-Ada-Gfp edited transcripts lacking the AUACCC motif do not show enrichment for other motifs

(**A**) *De novo* motif discovery analysis on transcripts that carried Khd4-Ada-Gfp editing sites but lacked the AUACCC motif. Scatter plot depicts the relative enrichment ratio (tested sequences vs. random genome background) against the percentage of tested sequences carrying the enriched motifs (grey). Enlarged region shows the sequence logo of the most represented motif. (**B**) Percentage of transcripts containing the UAGGCUUUGG motif in different transcript sets of the Venn diagram in Fig. 3B. Statistical significance was determined using Fisher's exact test. (**C**) Histogram illustrating the distribution of editing sites from the nearest UAGGCUUUGG motifs in transcripts specific to Khd4-Ada-Gfp (blue) compared to control-Ada (grey). (**D**) Positional maps of the AUACCC (top) and AGAUCU (bottom) motifs relative to the start (left panel) or stop codon (right panel) in Khd4-bound mRNAs (red) compared to all AUACCC-containing mRNAs (salmon). The transcript model on top shows the relative positions of the motifs in the 5´ UTR (5´; black), open reading frame (grey), and 3´ UTR (3´; black). (**E**) GO terms enrichment analysis of Khd4-bound mRNAs (g-SCS, P<0.05). Nodes (red) represent the significantly enriched GO terms, and their size corresponds to the number of genes associated with each term. The edges depict the overlap between genes associated with different GO terms. Highly similar GO terms are clustered and annotated according to the summarizing terms. GO term size is given below. Example genes corresponding to the GO terms GTPase regulator activity (GO:0030695) and small GTPase-mediated signal transduction (GO:0007264) are shown.

A

No.	UMAG_ID[a]	Annotation[b]	AUACCC[c]	GO term_ID[d]	Subcellular localization[e]
1	10152	cytokinesis protein Don1	5´UTR	0030695; 0007264	Cyotplasm
2	12272	Serine/threonine-protein kinase Smu1	5´UTR	0007264	Cyotplasm
3	06062	Rho-GAP domain-containing protein	5´UTR; ORF	0030695	Cyotplasm
4	00149	Adenylate cyclase	5´UTR; ORF	0030695; 0007264	Cyotplasm
5	01834	Uncharacterized protein	5´UTR, ORF	0030695	Cyotplasm
6	10461	SEC7 domain containing protein	ORF	0030695; 0007264	Cyotplasm
7	01378	Uncharacterized protein	ORF	0030695; 0007264	Cyotplasm
8	12185	DH domain-containing protein	ORF	0030695; 0007264	Cyotplasm
9	10305	Rab-GAP TBC domain-containing protein	ORF	0030695	Cyotplasm;Vacuole
10	15070	probable to GDP/GTP exchange factor Rom2p	ORF	0030695; 0007264	Cyotplasm
11	01161	adenylyl cyclase	ORF, 3´UTR	0030695; 0007264	Cyotplasm
12	04323	RING-type domain-containing protein	ORF, 3´UTR	0030695	Cyotplasm
13	10313	**Arl1**★	3´UTR	0007264	Cyotplasm;GA
14	02431	Ras-GAP domain containing protein	3´UTR	0030696	Cyotplasm
15	04352	probable MOB1 protein	3´UTR	0007264	Cyotplasm
16	11909	Putative GTP-binding protein	3´UTR	0007264	PM; Vacuole
17	00949	probable RAS GTPase-activating protein sar1	3´UTR	0030695; 0007264	Cyotplasm

GO:0030695 - GTPase regulator activity
GO:0007264- small GTPase mediated signal transduction
GA-Golgi apparatus; PM- Plasma membrane
a   UMAG_IDs of target mRNAs
b   *U. maydis* annotation according to PEDANT and Uniprot database
c   AUACCC motif position
d   GO-terms from enrichment analysis
e   predicted subcellular location
★   Example Khd4-bound mRNA targets from Fig. 3A

B

No.	UMAG_ID[a]	Annotation[b]	AUACCC[c]	Subcellular localization[e]
1	11514	Putative High-affinity glucose transporter	5´UTR	Vacuole
2	00987	Nucleoside diphosphatase	5´UTR	Vacuole; GA
3	10210	Copper transport protein	5´UTR	Vacuole; PM
4	00956	RGS domain-containing protein	5´UTR	Vacuole; PM
5	11352	Neutral ceramidase	5´UTR; ORF; 3´UTR	ER; Vacuole; GA; Secreted
6	04796	C2 domain-containing protein	5´ UTR; ORF	ER
7	12090	Elongation of fatty acids protein	5´UTR; ORF	ER
8	10305	Rab-GAP TBC domain-containing protein	ORF	Cytoplasm; Vacuole
9	01927	1-alkyl-2-acetylglycerophosphocholine esterase	ORF	Cytoplasm; ER
10	12181	Glycosyltransferase family 31 protein	ORF	GA
11	10916	Autophag-related protein 14	ORF	Cytoplasm; endosome; Vacuole
12	00003	golgi apparatus membrane protein	ORF; 3´UTR	PM; Vacuole
13	03569	GH16 domain-containing protein	ORF; 3´UTR	PM; Vacuole
14	02224	Palmitoyltransferase	ORF; 3´UTR	ER; Vacuole; GA
15	15053	DUF3971 domain-containing protein	ORF; 3´UTR	PM; Vacuole
16	11790	**Hok1**★	3´UTR	Cytoplasm; EE
17	10284	Putative vacuolar sorting protein HbrA	3´UTR	Cytoplasm; Vacuole
18	04579	PITH domain-containing protein	3´UTR	ER; Cytoplasm
19	02668	SUN domain-containing protein	3´UTR	ER
20	10313	**Arl1**★	3´UTR	Cytoplasm; GA
21	05729	PQ loop repeat protein	3´UTR	PM; Vacuole
22	04475	Protein kinase domain-containing protein	3´UTR	PM; Vacuole
23	11406	TLC domain-containing protein	3´UTR	ER
24	11909	Putative GTP-binding protein	3´UTR	PM; Vacuole
25	05167	Secreted protein	3´UTR	Secreted; ER
26	03283	DUF4149 domain-containing protein	3´UTR	ER
27	11418	**Vma21**★	3´UTR	ER
28	11017	related to CAP59 (required for capsule formation)	3´UTR	ER; Vacuole; GA

ER- Endoplasmic Reticulum; GA-Golgi apparatus; PM- Plasma membrane; EE- early endosome

Fig. S9. Khd4 targets are enriched for membrane trafficking regulators

(A) Table depicting Khd4-bound mRNAs enriched for GO terms, small GTPase-mediated signal transduction (GO:0007264), and GTPase regulator activity (GO:0030695). **(B)** Khd4-bound mRNAs are manually curated for subcellular localization to the endomembrane system.
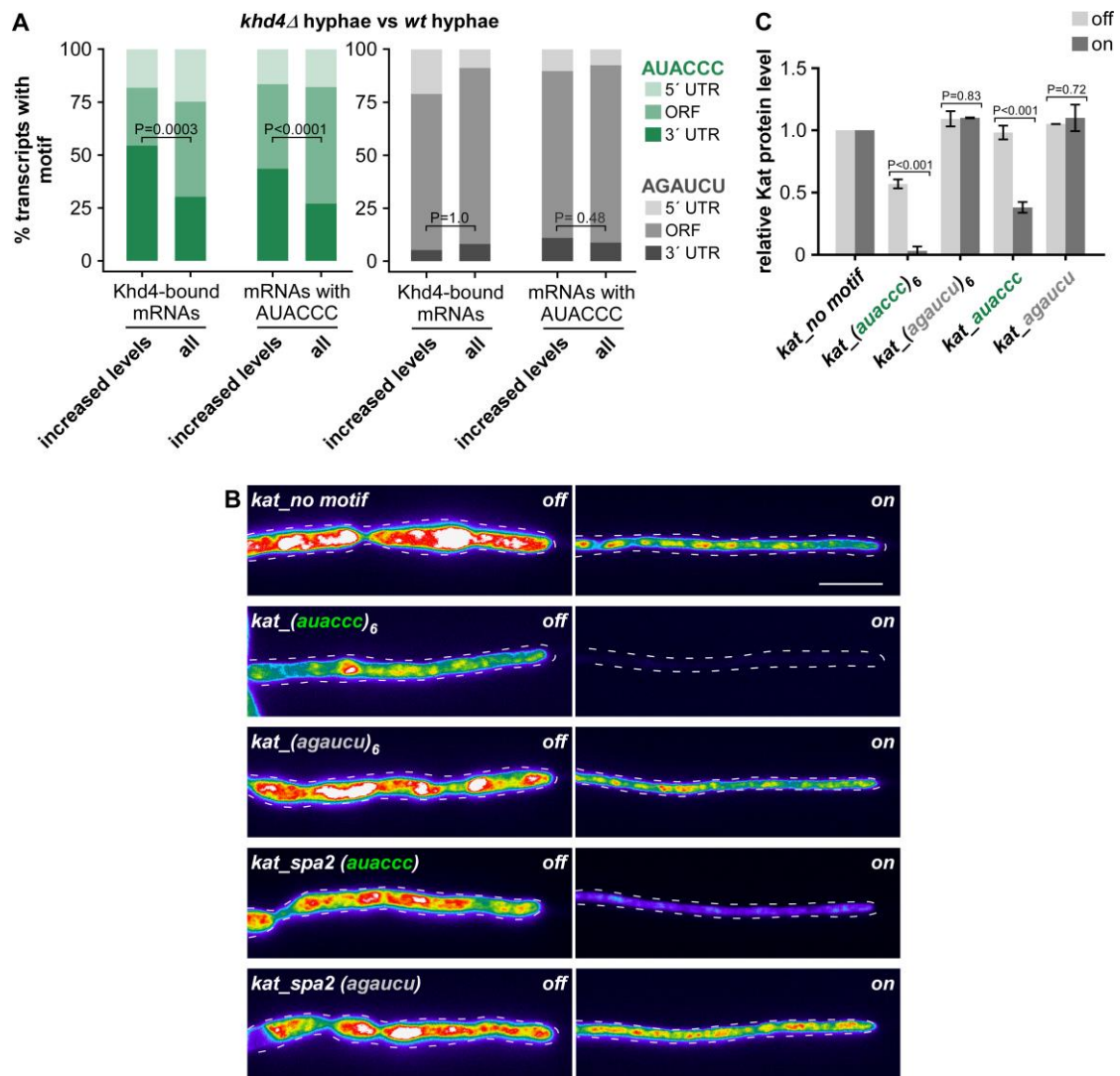
Fig. S10. The AUACCC motif in the 3' UTR determines protein levels

(A) Percentage of AUACCC (left; green) or AGAUCU (right; grey) motifs per transcript region (5´ UTR, ORF, 3´ UTR) for Khd4-bound mRNAs and mRNAs with AUACCC motifs that show increased expression levels in hyphae upon *khd4* deletion (*khd4Δ* hyphae vs. *wt* hyphae) in comparison to all mRNAs in the respective dataset. Statistical analysis was performed using Fisher's exact test. **(B)** Fluorescent micrographs in false color of hyphae (6 h.p.i.) constitutively expressing *kat* mRNA tethered to different 3´ UTR regions under Khd4-repressed off (left) and Khd4-induced on conditions (right) (*auaccc6* or *agaucu6*- 3´ UTR consisting of six repeats of the respective motifs; *kat_spa2 (auaccc)*- 36 nt long endogenous 3´ UTR sequence of *spa2* gene that contains a single AUACCC motif; *kat_spa2 (agaucu)*- 36 nt long endogenous 3´ UTR sequence of *spa2* gene that contains the mutated AUACCC motif; Kat- mKate2; scale bar: 10 μm). **(C)** Shown is the modified version of Fig. 4E. The Kat fluorescence levels measured in on (dark grey; Khd4-induced) and off conditions (light grey; Khd4-repressed) are shown relative to control Kat levels encoded by *kat_no motif*. Statistical significance between off and on conditions was compared using multiple unpaired Student's *t*-tests. (n=3 independent experiments; error bars: s.e.m.). The presence of six copies of the AUACCC motif in 3´ UTR leads to a stronger reduction in Kat fluorescence levels, even under Khd4-repressed off condition, highlighting the robust regulatory interplay between the tandem AUACCC repeats and basal Khd4 expression.
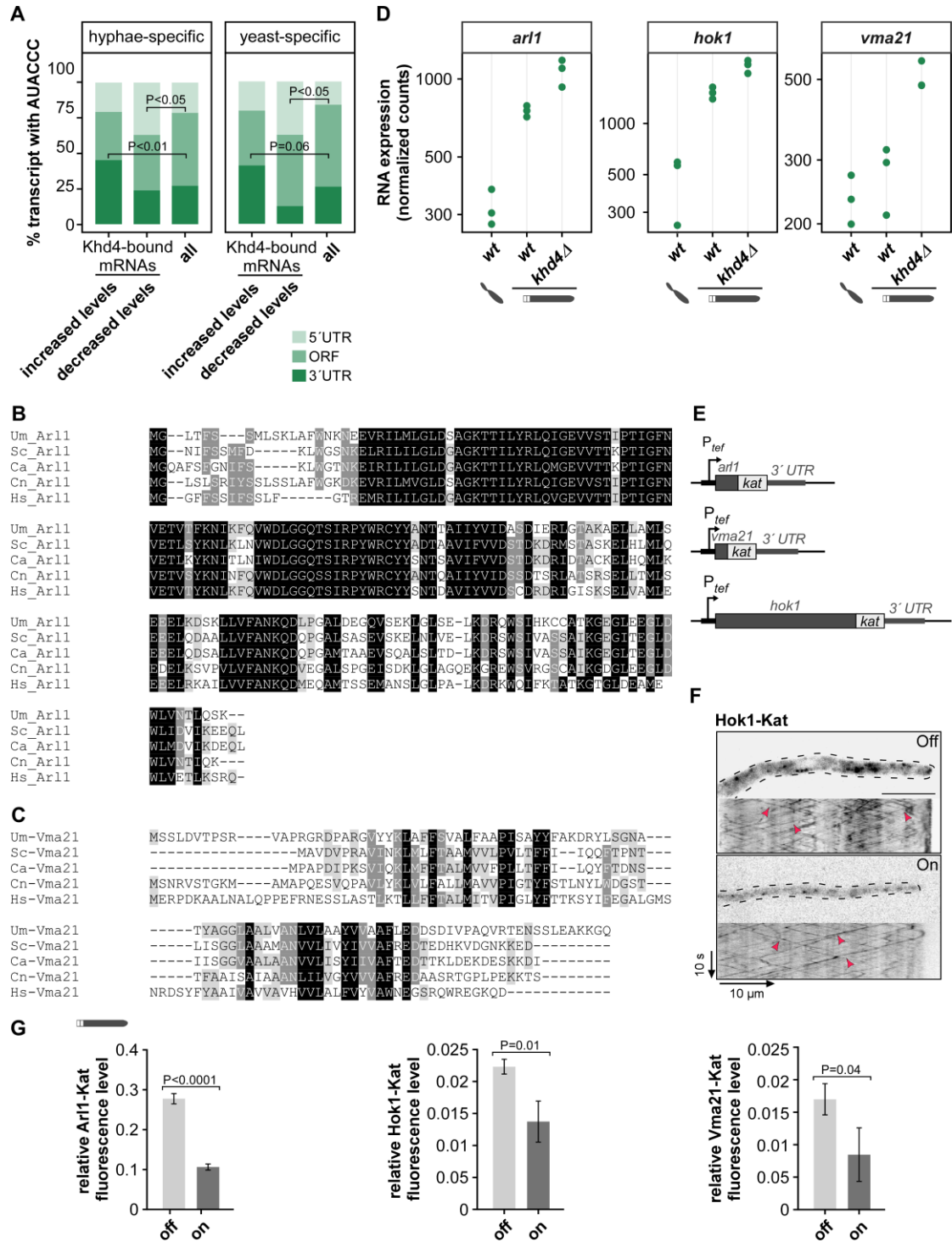
Fig. S11. Khd4 binding to the 3´ UTR AUACCC is crucial for determining the precise levels of mRNAs encoding membrane trafficking regulators

(**A**) Percentage of AUACCC motif per transcript region (5´ UTR, ORF, 3´ UTR) in hyphal-specific (left) and yeast-specific (right) Khd4-bound mRNAs that show increased or decreased expression levels in hyphae upon *khd4* deletion (*khd4Δ* hyphae vs. *wt* hyphae) in comparison to all mRNAs in the respective dataset (hyphal-specific or yeast-specific). Statistical analysis was carried out using Fisher's exact test. (**B**) Sequence alignments of Arl1 and (**C**) Vma21. *Um*_Arl1 from *U. maydis* (UMAG_10313), *Sc*_Arl1 from *S. cerevisiae* (NP_009723.3), *Ca*_Arl1 from *C. albicans* (XP_722675.1), *Cn*_Arl1 from *C. neoformans* (XP_012049462.1),

28

*Hs*_Arl1 from *Homo Sapiens* (NP_001168.1). Likewise, *Um*_Vma21 from *U. maydis* (UMAG_11418), *Sc*_ Vma21 from *S. cerevisiae* (NP_011619.3), *Ca*_ Vma21 from *C. albicans* (XP_019330812.1), *Cn*_ Vma21 from *C. neoformans* (XP_024513701.1), *Hs*_ Vma21 from *Homo Sapiens* (NP_001017980.1). **(D)** Plot showing mRNA expression levels (normalized RNA-seq read counts) of target mRNAs namely, *arl1*, *hok1,* and *vma21* in *wt* yeast, *wt* hyphae, and *khd4Δ* hyphae. Green dots represent the values from three biological replicates. **(E)** Ectopic expression constructs of target mRNAs, *arl1*, *vma21*, and *hok1*. ORFs of target mRNAs and the fluorescent tag, *kat* are shown in dark and light grey, respectively. The 3' UTR region (dark grey) was derived from the endogenous 500 bp sequence downstream of the respective target gene stop codon. The constructs were expressed ectopically using the constitutively active P_{tef} promoter. **(F)** Inverted fluorescent images and the corresponding kymographs of hyphal cells constitutively expressing Hok1-Kat in a genetic background of the arabinose inducible Khd4-GFP, under Khd4-repressed off (left) and Khd4-induced on (right) conditions. In the Khd4-repressed off condition, the Hok1-Kat signal was more pronounced on shuttling early endosomes. Red arrowheads indicate the processive signals. Scale bar: 10 µm. **(G)** Expression levels of target proteins in hyphal cells under Khd4-induced on and Khd4-repressed off conditions, measured by Kat fluorescent intensity. The fluorescence level relative to the constitutively expressed Kat control *(kat_no motif)* is given. Statistical evaluation of the relative fluorescent intensity between off and on conditions was performed using unpaired Student's *t*-test (n=3 independent experiments; error bars: s.e.m).
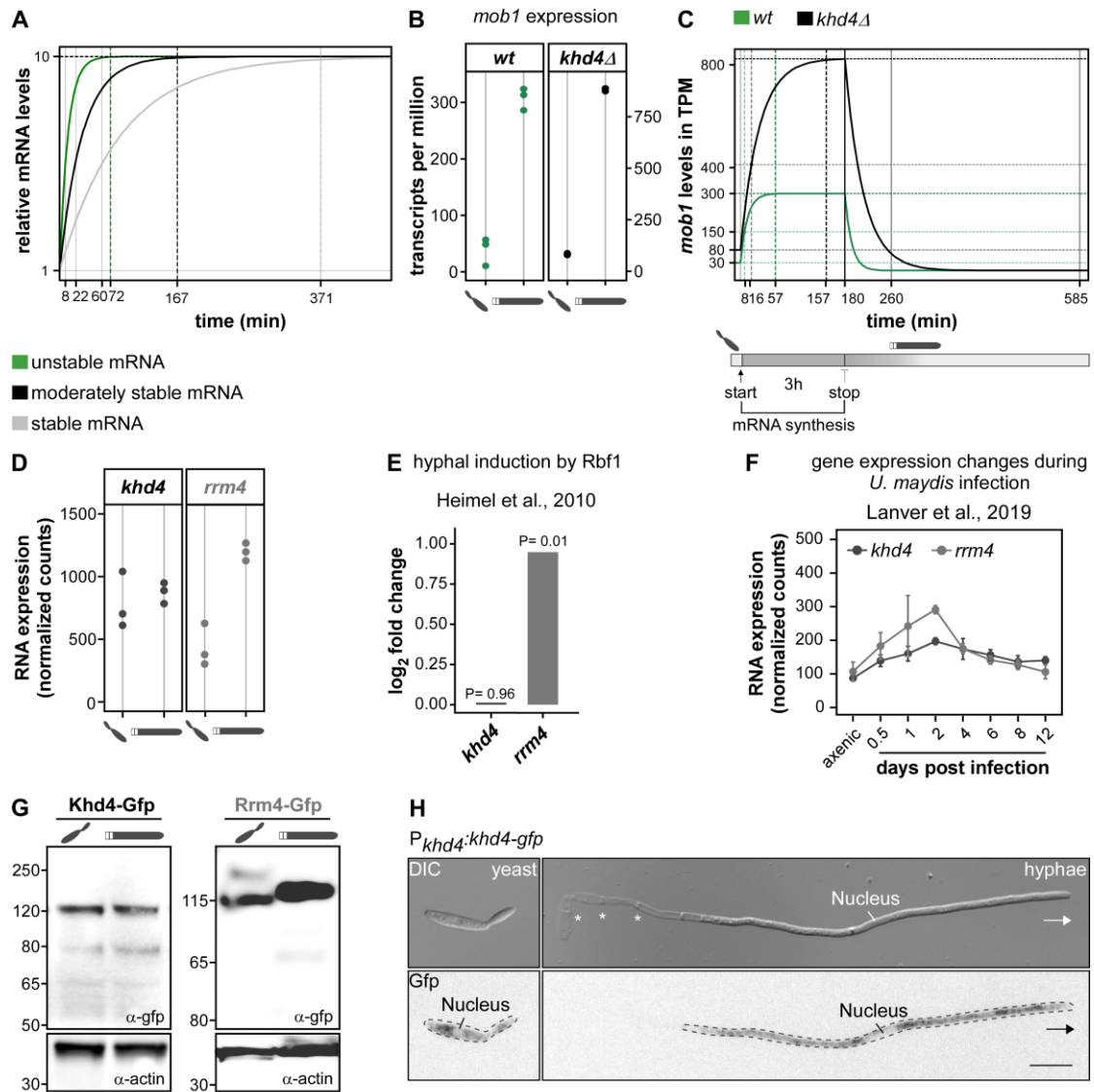
Fig. S12. Unstable mRNAs are crucial for rapid gene expression changes

(A) Single-compartment model describing induction kinetics of how exemplary mRNAs reach the same steady-state levels with different mRNA half-lives. The unstable mRNA reaches the new steady-state levels (10-fold increase) already after 72 min, compared to 167 min for moderately stable and >300 min for the stable mRNA. Green: Unstable mRNAs with rapid synthesis (0.87 transcripts/min) and short half-life ($t_{1/2}$ = 8 min, similar to *mob1* mRNA). Black: Moderately stable mRNAs with intermediate synthesis rate (0.3 transcripts/min) and half-life ($t_{1/2}$ = 22 min). Grey: Stable mRNA with slow synthesis (0.12 transcripts/min) and long half-life similar to *actin* mRNA ($t_{1/2}$ = 60 min). The half-life data is acquired from *S. cerevisiae* (6). The horizontal dashed line indicates the steady-state level (10-fold increase). The vertical dashed lines indicate the mRNA half-lives. **(B)** Steady-state levels of *mob1* in yeast and hyphal stages of wildtype (*wt,* green; left panel) and *khd4Δ* cells (black; right panel). The *mob1* levels are given in transcripts per million (TPM). The hyphal induction in wildtype cells causes a ~10-fold increase in *mob1* level. While the 10-fold increase persisted, the deletion of *khd4* caused elevated *mob1* levels in both yeast and hyphal cells. **(C)** Model-predicted induction kinetics and half-lives for *mob1* mRNA in *wt* and *khd4Δ* cells. Bottom: Schematic of *mob1* induction. The synthesis rate of *mob1* increases during hyphal morphogenesis, resulting in a 10-fold induction

measured in our RNA-seq. To visualize the transcriptional shutdown, we arbitrarily assumed that *mob1* transcription ceases after 3 hours, resulting in a return to its original steady-state level. Top: Changes in *mob1* steady-state levels in *wt* (green) and *khd4Δ* (black) cells following the switch from yeast to hyphae. Based on the single-component model, *mob1* mRNA reaches its steady-state level within 57 min of induction in *wt* cells. Moreover, the model predicts that *mob1* mRNA should be stabilized to a half-life of ~22 min in *khd4Δ* cells to account for the measured increase in *mob1* steady-state levels without altering the synthesis rate. The induction kinetics in *khd4Δ* cells are substantially delayed, reaching steady-state levels only after ~157 min. The same is observed after transcriptional shutdown, whereby *mob1* expression reverts to the original steady-state levels within ~80 min in *wt* cells vs. ~400 min in *khd4Δ* cells. The vertical dashed lines indicate the half-life of the corresponding mRNAs. The horizontal dashed lines show the half-maximal levels (light green, light grey for *wt* and *khd4Δ*, respectively) and new steady-state levels (green, black for *wt* and *khd4Δ*, respectively). **(D)** mRNA expression levels (normalized RNA-seq read counts) of *khd4* and *rrm4* in *wt* yeast and hyphal cells. Black and grey dots represent the count values of *khd4* and *rrm4* from n=3 biological replicates. **(E)** Changes in gene expression levels ($\log_2$-transformed fold change; microarray analysis (37)) for *khd4* (black) and *rrm4* (grey) after induction of the master regulator Rbf1 required for hyphae formation (37). Adjusted P-values from the gene expression analysis are shown on top. **(F)** Changes in gene expression for *khd4* and *rrm4* during pathogenic development of *U. maydis*. The time-course RNA-seq expression data presented here is acquired from (38). **(G)** Western blot analysis to examine the expression levels of endogenous Khd4 and Rrm4, which were tagged with Gfp at the C-terminus, in *wt* yeast and hyphal cells. Immunoblotting was performed using α-Gfp and α-Actin. The size of protein markers (kDa) is shown on the left (molecular weight of the proteins: Khd4- ~151 kDa, Rrm4- ~85 kDa, Gfp- ~27 kDa). **(H)** DIC (top) and fluorescence images (bottom) of AB33 yeast (left) and hyphae expressing endogenous Khd4 fused with Gfp at its C terminus (arrows and asterisks indicate growth direction and empty sections, respectively; scale bar: 10 µm).
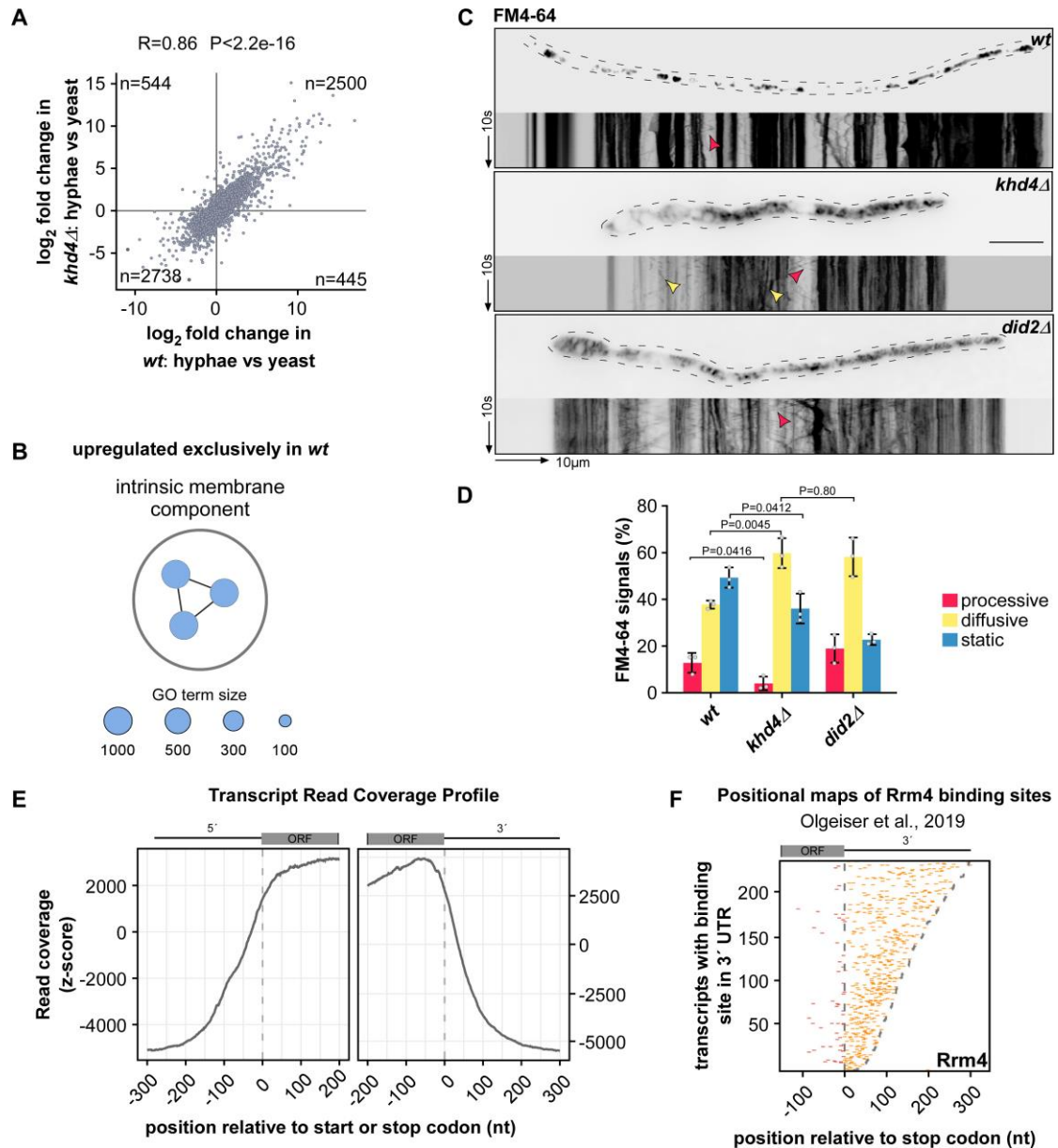
Fig. S13. Loss of Khd4 triggers defects in membrane trafficking dynamics

(A) Scatter plot comparing the $\log_2$-transformed fold change of genes in *wt* and *khd4Δ* cells upon hyphal induction (*wt*: hyphae vs. yeast and *khd4Δ*: hyphae vs. yeast, respectively). The number of data points in each quadrant is shown inside. (Pearson correlation coefficient R=0.86, P<2.26e-16). (B) Gene ontology (GO) terms that are significantly (P<0.05, multiple-testing correction with g: SCS algorithm) overrepresented in upregulated genes that are specific to *wt* cells (light blue) after hyphal induction (orange; >1.5-fold change, P<0.05, Benjamini-Hochberg corrections, >10 average normalized reads). The reference GO term sizes are given below. (C) Inverted micrographs (top panel) of AB33 hyphae derivatives (10 h.p.i.) after 25 min of FM4-64 staining. The corresponding kymograph is shown below. (top- wildtype; center- *khd4Δ*; bottom- *did2Δ*; processive and diffusive signals are indicated with red and yellow arrowheads, respectively; scale bar: 10 µm). (D) Bar chart depicting the amount of FM4-64 signals (%) in AB33-derived hyphal cells (>25 hyphal cells per strain; error bars: s.e.m.; grey dots represent independent experiments, n=3; signals were scored as processive (red) if the run length is >5 µm, diffusive (yellow) if the run length is <5 µm but >0 µm, static (blue) when the

run length is ~0 µm; unpaired Student's *t*-test). **(E)** Normalized read coverage in 5´ and 3´ UTR regions relative to start or stop codon for transcripts expressed in *U. maydis* hyphal cells (9.h.p.i.). The gene model on top shows the relative positions of the ORF and UTRs (5´, 3´- 5´ UTR, and 3´ UTR, respectively; black). Transcripts are ordered by increasing UTR length. **(F)** Positional maps of Rrm4 iCLIP binding sites relative to stop codon. The 234 randomly selected target transcripts are displayed, highlighting the Rrm4 binding sites (orange) within their 3´ UTR regions. The 3´ UTR region in these transcripts was annotated manually using RNA-seq data obtained from *U. maydis* hyphal cells (2). Grey dotted line depicts the borders of 3´ UTR (this figure is modified and reused from 2). Transcripts are ordered by decreasing UTR length.

4 Supporting Information Tables

Table S1: Description of *U. maydi*s strains used in this study

Strain name with code	locus	Progenitor strain	Short description
AB33 (UMa133)	*b*	FB2	*a2 Pnar: bW2 bE1,* expresses the heteromeric bW/bE transcription factor under the control of inducible P*nar1* promoter. Hyphal growth is induced by changing the nitrogen source.
AB33 khd4Δ (UMa482)	*khd4*	AB33	Carries *khd4* deletion
AB33 did2Δ (UMa934)	*did2*	AB33	Carries *did2* deletion
AB33 rrm4-gfp (UMa427)	*rrm4*	AB33	Expresses Rrm4 C-terminally fused to eGfp
AB33 khd4-gfp (UMa869)	*khd4*	AB33	Expresses Khd4 C-terminally fused to eGfp
AB33 P$_{crg1}$: rrm4-ada-gfp / rrm4Δ (UMa2805)	*ip^s*	AB33 rrm4Δ	Expresses Rrm4-Ada-Gfp fusion protein under the control of the arabinose-inducible P*crg1* promoter. The construct is ectopically integrated into the *ip^s* locus of the strain carrying *rrm4* deletion.
AB33 P$_{crg1}$: rrm4 -gfp / rrm4Δ (UMa2805)	*ip^s*	AB33 rrm4Δ	Expresses Rrm4- Gfp fusion protein under the control of the arabinose-inducible P*crg1* promoter. The construct is ectopically integrated into the *ip^s* locus of the strain carrying *rrm4* deletion.
AB33 P$_{crg1}$: khd4-ada-gfp / khd4Δ (UMa2988)	*ip^s*	AB33 khd4Δ	Expresses Khd4-Ada-Gfp fusion protein under the control of the arabinose-inducible P*crg1* promoter. The construct is ectopically integrated into the *ip^s* locus of the strain carrying *khd4* deletion.
AB33 P$_{crg1}$: khd4-gfp / khd4Δ (UMa2989)	*ip^s*	AB33 khd4Δ	Expresses Khd4-Gfp fusion protein under the control of the arabinose-inducible P*crg1* promoter. The construct is ectopically integrated into the *ip^s* locus of the strain carrying *khd4* deletion.
AB33 P$_{crg1}$: kat-ada-gfp (UMa3083)	*ip^s*	AB33	Expresses Kat-Ada-Gfp fusion protein under the control of the arabinose-inducible P*crg1* promoter. The construct is ectopically integrated into the *ip^s* locus.

AB33 P$_{crg1}$: khd4-gfp / khd4Δ / upp3Δ (UMa3138)	*upp3*	AB33 P$_{crg1}$: khd4-gfp / khd4Δ	*upp3* deletion in the strain that carries *khd4* deletion and ectopically expresses *khd4-gfp* under the control of the arabinose-inducible P$_{crg1}$ promoter
AB33 P$_{crg1}$: khd4- ada-gfp / khd4Δ / upp3Δ (UMa3290)	*upp3*	AB33 P$_{crg1}$: khd4-ada-gfp / khd4Δ	*upp3* deletion in the strain that carries *khd4* deletion and ectopically expresses *khd4-ada-gfp* under the control of arabinose inducible P$_{crg1}$ promoter.
AB33 P$_{tef}$: kat_(auaccc)$_6$ / P$_{crg1}$: khd4-ada-gfp / khd4Δ / upp3Δ (UMa3293)	*upp3*	AB33 P$_{crg1}$: khd4-ada-gfp / khd4Δ / upp3Δ	Expression of *mkate2 (kat)* ORF containing six tandem repeats of the *auaccc* motif in its 3´ UTR using the constitutively active P$_{tef}$ promoter. The construct is integrated into the *upp3Δ* locus of the strain ectopically expressing *khd4-ada-gfp* under the control of the P$_{crg1}$ promoter and carrying *khd4* deletion.
AB33 P$_{tef}$: kat_(auaccc)$_6$ / P$_{crg1}$: khd4-gfp / khd4Δ / upp3Δ (UMa3140)	*upp3*	AB33 P$_{crg1}$: khd4-gfp / khd4Δ / upp3Δ	Expression of *kat* ORF containing six tandem repeats of the *auaccc* motif in its 3´ UTR using the constitutively active P$_{tef}$ promoter. The construct is integrated into the *upp3Δ* locus of the strain expressing *khd4-gfp* ectopically under the control of the P$_{crg1}$ promoter and carrying the *khd4* deletion.
AB33 P$_{tef}$: kat_no motif / P$_{crg1}$: khd4-gfp / khd4Δ / upp3Δ (UMa3139)	*upp3*	AB33 P$_{crg1}$: khd4-gfp / khd4Δ / upp3Δ	Expression of *kat* ORF containing no motif in its 3´ UTR using the constitutively active P$_{tef}$ promoter. The construct is integrated into the *upp3Δ* locus of the strain expressing *khd4-gfp* ectopically under the control of the P$_{crg1}$ promoter and carrying the *khd4* deletion.
AB33 P$_{tef}$: kat_(agaucu)$_6$ / P$_{crg1}$: khd4-gfp / khd4Δ / upp3Δ (UMa3141)	*upp3*	AB33 P$_{crg1}$: khd4-gfp / khd4Δ / upp3Δ	Constitutively expresses the *kat* ORF containing six tandem repeats of the *agaucu* motif in its 3´ UTR under the control of the P$_{tef}$ promoter. The construct is integrated into the *upp3Δ* locus of the strain expressing *khd4-gfp* ectopically under the control of the P$_{crg1}$ promoter and carrying the *khd4* deletion.
AB33 P$_{tef}$: kat_(auaccc) / P$_{crg1}$: khd4-gfp /khd4Δ/upp3Δ (UMa3238)	*upp3*	AB33 P$_{crg1}$: khd4-gfp / khd4Δ / upp3Δ	Expression of the *kat* ORF carrying 36 nt 3´ UTR sequences from *spa2* gene which contains one *auaccc* motif. Constitutive expression was carried out using the P$_{tef}$

			promoter. The construct is integrated into the *upp3Δ* locus of the strain expressing *khd4-gfp* ectopically under the control of the P*crg1* promoter and carrying the *khd4* deletion.
AB33 P*tef*: kat_(agaucu) / P*crg1*: khd4-gfp /khd4Δ/upp3Δ (UMa3239)	*upp3*	AB33 P*crg1*: khd4-gfp / khd4Δ / upp3Δ	Expression of the *kat* ORF carrying 36 nt 3´ UTR sequences from *spa2* gene where *auaccc* sequence is mutated to *agaucu*. Constitutively active P*tef* promoter was used for expression. The construct is integrated into the *upp3Δ* locus of the strain expressing *khd4-gfp* ectopically under the control of the P*crg1* promoter and carrying the *khd4* deletion.
AB33 P*tef*: arl1-kat_ arl1 3´ UTR / P*crg1*: khd4-gfp /khd4Δ/upp3Δ (UL0008)	*upp3*	AB33 P*crg1*: khd4-gfp / khd4Δ / upp3Δ	Constitutive expression of target mRNA *arl1* fused with *kat* using P*tef* promoter. 500 nt long endogenous sequence downstream of the *arl1* stop codon was used as the 3´ UTR region The construct is integrated into the *upp3Δ* locus of the strain expressing *khd4-gfp* ectopically under the control of the P*crg1* promoter and carrying the *khd4* deletion.
AB33 P*tef*: hok1-kat_ hok1 3´ UTR / P*crg1*: khd4-gfp /khd4Δ/upp3Δ (UL0012)	*upp3*	AB33 P*crg1*: khd4-gfp / khd4Δ / upp3Δ	Constitutive expression of target mRNA *hok1* fused with *kat* using P*tef* promoter. 500 nt long endogenous sequence downstream of the *hok1* stop codon was used as the 3´ UTR region. The construct is integrated into the *upp3Δ* locus of the strain expressing *khd4-gfp* ectopically under the control of the P*crg1* promoter and carrying the *khd4* deletion.
AB33 P*tef*: vma21-kat_ vma21 3´ UTR / P*crg1*: khd4-gfp /khd4Δ/upp3Δ (UL0009)	*upp3*	AB33 P*crg1*: khd4-gfp / khd4Δ / upp3Δ	Constitutive expression of target mRNA *vma21* fused with *kat* using P*tef* promoter. 500 nt long endogenous sequence downstream of the *vma21* stop codon was used as the 3´ UTR region. The construct is integrated into the *upp3Δ* locus of the strain expressing *khd4-gfp* ectopically under the control of the P*crg1* promoter and carrying the *khd4* deletion.

UMa & UL: internal strain reference number; Kat: mKate2, a monomeric form of the red fluorescent protein; eGfp- enhanced Gfp.

Table S2: Generation of *U. maydis* strains used in this study

Strain name	Relevant genotypes	Strain code	Progenitor strain	Transformed plasmid	Locus	References
AB33	*a2 Pnar:bW2 bE1*	UMa133	FB2	pAB33	*b*	(9)
AB33 khd4Δ	*khd4*	UMa482	AB33	pUMa1142	*khd4*	(39)
AB33 did2Δ	*did2*	UMa934	AB33	pUMa1699	*did2*	(40)
AB33 rrm4-gfp	*rrm4*	UMaxxx	AB33	pUMa496	*rrm4*	(41)
AB33 khd4-gfp	*khd4*	UMa869	AB33	pUMa1484	*khd4*	(39)
AB33 P$_{crg1}$: rrm4-ada-gfp / rrm4Δ	*rrm4Δ / rrm4-ada-gfp*	UMa2805	AB33 rrm4Δ	pUMa3975	*ip^s*	This study
AB33 P$_{crg1}$: rrm4- gfp / rrm4Δ	*rrm4Δ / rrm4- gfp*	UMa2807	AB33 rrm4Δ	pUMa3981	*ip^s*	This study
AB33 P$_{crg1}$: khd4-ada-gfp / khd4Δ	*khd4Δ / khd4-ada-gfp*	UMa2988	AB33 khd4Δ	pUMa4057	*ip^s*	This study
AB33 P$_{crg1}$: khd4-gfp / khd4Δ	*khd4Δ / khd4-ada-gfp*	UMa2989	AB33 khd4Δ	pUMa4080	*ip^s*	This study
AB33 P$_{crg1}$: kat-ada-gfp	*kat-ada-gfp*	UMa3083	AB33	pUMa4290	*ip^s*	This study
AB33 P$_{crg1}$: khd4-gfp / khd4Δ / upp3Δ	*khd4Δ / khd4-gfp / upp3Δ*	UMa3138	AB33 P$_{crg1}$: khd4-gfp / khd4Δ	pUMa4378	*upp3*	This study
AB33 P$_{crg1}$: khd4- ada-gfp / khd4Δ / upp3Δ	*khd4Δ / khd4-ada-gfp / upp3Δ*	UMa3290	AB33 P$_{crg1}$: khd4-ada-gfp / khd4Δ	pUMa4378	*upp3*	This study

AB33 P_{tef}: kat_(auaccc)₆ / P_{crg1}: khd4-ada-gfp / khd4Δ / upp3Δ	*khd4Δ / khd4-ada-gfp / upp3Δ*	UMa3293	AB33 P_{crg1}: khd4-ada-gfp / khd4Δ / upp3Δ	pUMa4385	*upp3*	This study
AB33 P_{tef}: kat_(auaccc)₆ / P_{crg1}: khd4-gfp / khd4Δ / upp3Δ	*khd4Δ / khd4-gfp / upp3Δ*	UMa3140	AB33 P_{crg1}: khd4-gfp / khd4Δ / upp3Δ	pUMa4385	*upp3*	This study
AB33 P_{tef}: kat_no motif / P_{crg1}: khd4-gfp / khd4Δ / upp3Δ	*khd4Δ / khd4-gfp / upp3Δ*	UMa3139	AB33 P_{crg1}: khd4-gfp / khd4Δ / upp3Δ	pUMa4383	*upp3*	This study
AB33 P_{tef}: kat_(agaucu)₆ / P_{crg1}: khd4-gfp / khd4Δ / upp3Δ	*khd4Δ / khd4-gfp / upp3Δ*	UMa3141	AB33 P_{crg1}: khd4-gfp / khd4Δ / upp3Δ	pUMa4384	*upp3*	This study
AB33 P_{tef}: kat_(auaccc) / P_{crg1}: khd4-gfp / khd4Δ / upp3Δ	*khd4Δ / khd4-gfp / upp3Δ*	UMa3238	AB33 P_{crg1}: khd4-gfp / khd4Δ / upp3Δ	pUMa4531	*upp3*	This study
AB33 P_{tef}: kat_(agaucu) / P_{crg1}: khd4-gfp / khd4Δ / upp3Δ	*khd4Δ / khd4-gfp / upp3Δ*	UMa3239	AB33 P_{crg1}: khd4-gfp / khd4Δ / upp3Δ	pUMa4532	*upp3*	This study
AB33 P_{tef}: arl1-kat_ arl1 3´ UTR / P_{crg1}: khd4-	*khd4Δ / khd4-gfp / upp3Δ / arl1-kat*	UL0008	AB33 P_{crg1}: khd4-gfp /	pUL0007	*upp3*	This study

gfp / khd4Δ / upp3Δ			khd4Δ / upp3Δ			
AB33 P_{tef}: hok1-kat_ hok1 3´ UTR / P_{crg1}: khd4-gfp / khd4Δ / upp3Δ	*khd4Δ / khd4-gfp / upp3Δ / hok1-kat*	UL0012	AB33 P_{crg1}: khd4-gfp / khd4Δ / upp3Δ	pUL0011	*upp3*	This study
AB33 P_{tef}: vma21-kat_ vma21 3´ UTR P_{crg1}: khd4-gfp khd4Δ / upp3Δ	*khd4Δ / khd4-gfp / upp3Δ / vma21 -kat*	UL0009	AB33 P_{crg1}: khd4-gfp / khd4Δ / upp3Δ	pUL0008	*upp3*	This study

UMa & UL: internal strain reference number; pUMa & pUL: internal plasmid reference number.

Table S3: Description of plasmids used for strain generation in this study

Plasmid name	Plasmid code	Resistance cassette	Short description
p P_{crg1}: Rrm4-Ada-Gfp (CbxR)	pUMa3975	CbxR (for integration into *ip* locus)	Plasmid for ectopic integration and expression of Rrm4-Ada-Gfp. The 2379 bp *rrm4*-ORF is fused C-terminally to the 1200 bp *adar* catalytic domain (Ada) with three repeats of GGGGS linker in between, followed by eGfp fusion. The construct is under the control of arabinose inducible P*crg1* promoter and flanked by the T$_{nos}$-terminator.
p P_{crg1}: Rrm4-Gfp (CbxR)	pUMa3981	CbxR (for integration into *ip* locus)	Plasmid for ectopic integration and expression of Rrm4-Gfp. The 2379 bp *khd4*-ORF is fused C-terminally with eGfp. The construct is flanked upstream and downstream by the arabinose inducible P*crg1* promoter and the T$_{nos}$-terminator, respectively.
p P_{crg1}: Khd4-Ada-Gfp (CbxR)	pUMa4057	CbxR (for integration into *ip* locus)	Plasmid for ectopic integration and expression of Khd4-Ada-Gfp. The 4282 bp *khd4*-ORF is fused C-terminally to the 1200 bp *adar* catalytic domain (Ada) with three repeats of GGGGS linker in between, followed by eGfp fusion. The construct is under the control of arabinose inducible P*crg1* promoter and flanked by the T$_{nos}$-terminator.
p P_{crg1}: Khd4-Gfp (CbxR)	pUMa4080	CbxR (for integration into *ip* locus)	Plasmid for ectopic integration and expression of Khd4-Gfp. The 4282 bp *khd4*-ORF is fused C-terminally with eGfp. The construct is flanked upstream and downstream by the arabinose inducible P*crg1* promoter and the T$_{nos}$-terminator, respectively.
p P_{crg1}: Kat-Ada-Gfp (CbxR)	pUMa4290	CbxR (for integration into *ip* locus)	Plasmid for ectopic integration and expression of Kat-Ada-Gfp. Like p P*crg1*: Khd4-Ada-Gfp (CbxR) but *khd4*-ORF was replaced with *kat*-ORF.

p Upp3Δ (G418R)	pUMa4378	G418R (Sfi1-insert of pMF1-g)	Plasmid used for *upp3* deletion. The G418R cassette is flanked upstream by 1.5 kb and downstream by 1.9kb of the immediate genomic region flanking *upp3*. The resistance cassette is derived from pMF1-g. (11, 35)
p P$_{tef}$: Kat_(AUACCC)$_6$ (NatR)	pUMa4385	NatR (Sfi1-insert of pMF-1n)	Plasmid for the ectopic expression of Kat reporter at *upp3Δ* locus. Six tandem repeats of the *auaccc* motif were placed at the 3´ UTR region of *kat*-ORF and expressed under the control of a constitutively active P$_{tef}$ promoter. The construct contains a T$_{nos}$ terminator, and a nourseothricin-resistance cassette and is flanked by upstream and downstream regions of the *upp3Δ* locus for homologous recombination.
p P$_{tef}$: Kat (NatR)	pUMa4383	NatR (Sfi1-insert of pMF-1n)	Plasmid for the ectopic expression of Kat reporter at *upp3Δ* locus. Like p P$_{tef}$: Kat_(AUACCC)$_6$ (NatR) but contains no specific motif in the 3´ UTR region The *kat*-ORF is immediately followed by a T$_{nos}$ terminator. Reporter expression is carried out by the constitutively active P$_{tef}$ promoter. The construct contains a nourseothricin-resistance cassette and is flanked by upstream and downstream regions of the *upp3Δ* locus for homologous recombination.
p P$_{tef}$: Kat_(AGAUCU)$_6$ (NatR)	pUMa4384	NatR (Sfi1-insert of pMF-1n)	Plasmid for the ectopic expression of Kat reporter at *upp3Δ* locus. Like p P$_{tef}$: Kat_(AUACCC)$_6$ (NatR) but contains six tandem repeats of *agaucu* motif in the 3´ UTR region Reporter expression is carried out by the constitutively active P$_{tef}$ promoter. The construct contains a T$_{nos}$ terminator and a nourseothricin-resistance cassette and is flanked by upstream and downstream regions of the *upp3Δ* locus for homologous recombination.
p P$_{tef}$: Kat_Spa2 short (AUACCC) (NatR)	pUMa4531	NatR (Sfi1-insert of pMF-1n)	Plasmid for the ectopic expression of Kat reporter at *upp3Δ* locus. Like p P$_{tef}$: Kat_(AUACCC)$_6$ (NatR) but consists of

			36 nt 3´ UTR sequence from *spa2* gene, containing one *auaccc* motif, in its 3´ UTR region. Reporter expression is carried out by the constitutively active P$_{tef}$ promoter. The construct contains a T$_{nos}$ terminator and a nourseothricin-resistance cassette and is flanked by upstream and downstream regions of the *upp3Δ* locus for homologous recombination.
p P$_{tef}$: Kat_Spa2 short (AGAUCU) (NatR)	pUMa4532	NatR (Sfi1-insert of pMF-1n)	Plasmid for the ectopic expression of Kat reporter at *upp3Δ* locus. Like p P$_{tef}$: Kat_Spa2 short (AUACCC) (NatR) but the *auaccc* motif is mutated to *agaucu*. Reporter expression is carried out by the constitutively active P$_{tef}$ promoter. The construct contains a T$_{nos}$ terminator and a nourseothricin-resistance cassette and is flanked by upstream and downstream regions of the *upp3Δ* locus for homologous recombination.
p P$_{tef}$: Arl1-Kat_3´ UTR arl1 (NatR)	pUL0007	NatR (Sfi1-insert of pMF-1n)	Plasmid expressing target mRNA *arl1* ectopically at *upp3Δ* locus. The 739 bp long *arl1*-ORF is fused C-terminally to Kat and expressed under the control of the constitutive P$_{tef}$ promoter. ~ 500 bp long endogenous sequence downstream of the *arl1* stop codon was used as the 3´ UTR region. The construct contains a T$_{nos}$-terminator and a nourseothricin-resistance cassette and is flanked by upstream and downstream regions of the *upp3Δ* locus for homologous recombination.
p P$_{tef}$: Hok1-Kat_3´ UTR hok1 (NatR)	pUL0011	NatR (Sfi1-insert of pMF-1n)	Plasmid expressing target mRNA *hok1* ectopically at *upp3Δ* locus. The 2814 bp long *hok1*-ORF is fused C-terminally to Kat and expressed under the control of the constitutive P$_{tef}$ promoter. ~ 500 bp long endogenous sequence downstream of *hok1* stop codon was used as the 3´ UTR region. The construct contains a T$_{nos}$-terminator and a nourseothricin-resistance cassette and is flanked by upstream and

			downstream regions of the *upp3Δ* locus for homologous recombination.
p P$_{tef}$: Vma21-Kat_3´ UTR vma21 (NatR)	pUL0008	NatR (Sfi1-insert of pMF-1n)	Plasmid expressing target mRNA *arl1* ectopically at *upp3Δ* locus. The 385 bp long *vma21*-ORF is fused C-terminally to Kat and expressed under the control of the constitutive P$_{tef}$ promoter. A 500 bp long endogenous sequence downstream of the *vma21* stop codon was used as the 3´ UTR region. The construct contains a T$_{nos}$-terminator and a nourseothricin-resistance cassette and is flanked by upstream and downstream regions of the *upp3Δ* locus for homologous recombination.

pUMa & pUL: internal plasmid reference number; Kat: mKate2, a monomeric form of the red fluorescent protein; eGfp: enhanced Gfp.

Table S4: Oligos used in this study

Designation	Nucleotide sequence (5' → 3')	Remarks
oUM27	AATAGGCCTGAGTGGCCATGGCCGAATCGATTTACG	*rrm4-fwd*
oUM573	CGCGGCCTGAGTGGCCATGGATTTCTACTCGACGTCCTTC	*khd4- fwd*
oUM574	GTAATAGGCCGCGTTGGCCGCCCGGTCAAAAGCGAGTTGAG	*khd4- rev*
oUM420	CATATAGGGATTCTGCCAGTCCGAACTC	*ada- rev*
oAB292	CGGAGGCGGTGGTTCCGGTGGCGGAGGATCGGGAGGTGGCGGTTCGTC	*GGGGS linker-fwd*
oAB293	CATGGACGAACCGCCACCTCCCGATCCTCCGCCACCGGAACCACCGCCTCCGGTAC	*GGGGS linker-rev*
oRL1385	CACCATATGGTGAGCAAGGGCGAGGAGC	*gfp- fwd*
oAB1	GCAAGGCCTGAGTGGCCATGGTGTCGGAGCTCATC	*kat- fwd*
oAB2	GTCTGGCCGCGTTGGCCCTCATATGGCGGTGACCG	*kat- rev*
oMB611	GATGCTCTTCCGTGCCATGGTGTCGGAGCTCATC	*kat reporter- fwd*
oAB222	GGCGCGCCTATAGTTAACGCTATCAGGCGTAGTCGGGCACGTCGTAAG	*kat reporter- rev*
oAB232	AACATACCCATACCCATACCCATACCCATACCCATACCCGG	*(auaccc)6- fwd*
oAB233	CGCGCCGGGTATGGGTATGGGTATGGGTATGGGTATGGGTATGGTATGTT	*(auaccc)6- rev*
oAB234	AACAGATCTAGATCTAGATCTAGATCTAGATCTAGATCTGG	*(agaucu)6-- fwd*
oAB235	CGCGCCAGATCTAGATCTAGATCTAGATCTAGATCTAGATCTGTT	*(agaucu)6- rev*
oAB531	AACCGTCAATCACGAATGATACCCACCTTGTCACCCGAGGG	*spa2 short (auaccc)- fwd*
oAB532	CGCGCCCTCGGGTGACAAGGTGGGTATCATTCGTGATTGACGGTT	*spa2 short (auaccc)- rev*
oAB533	AACCGTCAATCACGAATGAGATCTACCTTGTCACCCGAGGG	*spa2 short (agaucu)-fwd*

oAB534	CGCGCCCTCGGGTGACAAGGTAGATCTCATTCGTGATTGACGGTT	*spa2 short (agaucu)-rev*
oCD81	GCTGGCAATTGATGGGTCTCACATTCTCGTC	*arl1- fwd*
oCD82	GCGCCGACTAGTCTTGCTTTGCAATGTGTTG	*arl1- rev*
oCD192	GCGGCTATGTTAACTCCATTCGAGACCTCCGATAC	*3´ UTR (arl1) - fwd*
oCD193	AGTCATGGCGCGCCTGCATTGTCTACCTGTGCTGAAG	*3´ UTR (arl1) - rev*
oCD208	GCCGATCAATTGATGTCGGACACGCATGACCC	*hok1- fwd*
oCD209	ATCGTAACTAGTCCTGCGACTAGCGAGCTGC	*hok1- rev*
oCD210	GGGCGGCGGTTAACTGTCGGAACCCTTTTTTATATACC	*3´ UTR (hok1) - fwd*
oCD211	GATCTAGGCGCGCCCACCTTTACCACCAACTAC	*3´ UTR (hok1) - rev*
oCD83	GAGCGCAATTGATGTCAAGCCTGGATGTG	*vma21- fwd*
oCD84	GCGGTCACTAGTTTGACCTTTCTTCGCCTCAAGACTG	*vma21- rev*
oCD194	GCTACGGTTAACGTAAGGAACATGACGAAGCAGG	*3´ UTR (vma21) - fwd*
oCD195	ACTATAGGCGCGCCTGTGGGAAGTGACACTGGTG	*3´ UTR (vma21) - rev*
oCD483	GACAAGGAAACCTACGTCGAG	*kat-RT-qPCR- fwd*
oCD484	TAGAGCGGACCCTGCATA	*kat-RT-qPCR- rev*
oCD485	GTTCCGCGAGACCATTCTTA	*pgk1-RT-qPCR- fwd*
oCD486	CCGGCAAAGTTGTCAAACTC	*pgk1-RT-qPCR- rev*

Fwd-forward; Rev-reverse.

5   Supporting Information References

1.   K. Müntjes, S. K. Devan, A. S. Reichert, M. Feldbrügge, Linking transport and translation of mRNAs with endosomes and mitochondria. *EMBO Rep* **22**, e52445 (2021).

2.   L. Olgeiser *et al.*, The key protein of endosomal mRNP transport Rrm4 binds translational landmark sites of cargo mRNAs. *EMBO Rep* **20** (2019).

3.   J. König *et al.*, The fungal RNA-binding protein Rrm4 mediates long-distance transport of *ubi1* and *rho3* mRNAs. *Embo j* **28**, 1855-1866 (2009).

4.   J. L. Hargrove, F. H. Schmidt, The role of mRNA and protein stability in gene expression. *Faseb j* **3**, 2360-2370 (1989).

5.   E. J. White, G. Brewer, G. M. Wilson, Post-transcriptional control of gene expression by AUF1: mechanisms, physiological targets, and regulation. *Biochim Biophys Acta* **1829**, 680-688 (2013).

6.   C. Miller *et al.*, Dynamic transcriptome analysis measures rates of mRNA synthesis and decay in yeast. *Mol Syst Biol* **7**, 458 (2011).

7.   A. Brachmann, J. König, C. Julius, M. Feldbrügge, A reverse genetic approach for generating gene replacement mutants in *Ustilago maydis*. *Mol Genet Genomics* **272**, 216-226 (2004).

8.   M. Terfrüchte *et al.*, Applying Unconventional Secretion in *Ustilago maydis* for the Export of Functional Nanobodies. *Int J Mol Sci* **18**, 937 (2017).

9.   A. Brachmann, G. Weinzierl, J. Kämper, R. Kahmann, Identification of genes in the bW/bE regulatory cascade in *Ustilago maydis*. *Mol Microbiol* **42**, 1047-1063 (2001).

10.   G. Loubradou, A. Brachmann, M. Feldbrügge, R. Kahmann, A homologue of the transcriptional repressor Ssn6p antagonizes cAMP signalling in *Ustilago maydis*. *Mol Microbiol* **40**, 719-730 (2001).

11.   P. Sarkari *et al.*, Improved expression of single-chain antibodies in *Ustilago maydis*. *J Biotechnol* **191**, 165-175 (2014).

12.   A. Kuttan, B. L. Bass, Mechanistic insights into editing-site specificity of ADARs. *Proc Natl Acad Sci U S A* **109**, E3295-3304 (2012).

13.   A. C. McMahon *et al.*, TRIBE: Hijacking an RNA-Editing Enzyme to Identify Cell-Specific Targets of RNA-Binding Proteins. *Cell* **165**, 742-753 (2016).

14.   W. Xu, R. Rahman, M. Rosbash, Mechanistic implications of enhanced editing by a HyperTRIBE RNA-binding protein. *Rna* **24**, 173-182 (2018).

15.   D. Shcherbo *et al.*, Far-red fluorescent tags for protein imaging in living tissues. *Biochem J* **418**, 567-574 (2009).

16.   J. Kämper *et al.*, Insights from the genome of the biotrophic fungal plant pathogen *Ustilago maydis*. *Nature* **444**, 97-101 (2006).

17.   R. Rahman, W. Xu, H. Jin, M. Rosbash, Identification of RNA-binding protein targets with HyperTRIBE. *Nat Protoc* **13**, 1829-1849 (2018).

18.   A. M. Bolger, M. Lohse, B. Usadel, Trimmomatic: a flexible trimmer for Illumina sequence data. *Bioinformatics* **30**, 2114-2120 (2014).

19.   A. Dobin *et al.*, STAR: ultrafast universal RNA-seq aligner. *Bioinformatics* **29**, 15-21 (2013).

20.   V. Thumuluri, J. J. Almagro Armenteros, A. R. Johansen, H. Nielsen, O. Winther, DeepLoc 2.0: multi-label subcellular localization prediction using protein language models. *Nucleic Acids Res* **50**, W228-234 (2022).

21.   D. Binns *et al.*, QuickGO: a web-based tool for Gene Ontology searching. *Bioinformatics* **25**, 3045-3046 (2009).

22.   R. P. Huntley *et al.*, The GOA database: gene Ontology annotation updates for 2015. *Nucleic Acids Res* **43**, D1057-1063 (2015).

23.   C. E. Grant, T. L. Bailey, XSTREME: Comprehensive motif analysis of biological sequence datasets. *bioRxiv* 10.1101/2021.09.02.458722, 2021.2009.2002.458722 (2021).

24.   E. Afgan *et al.*, The Galaxy platform for accessible, reproducible and collaborative biomedical analyses: 2018 update. *Nucleic Acids Res* **46**, W537-W544 (2018).

25.   S. Anders, P. T. Pyl, W. Huber, HTSeq—a Python framework to work with high-throughput sequencing data. *Bioinformatics* **31**, 166-169 (2014).

26.   M. I. Love, W. Huber, S. Anders, Moderated estimation of fold change and dispersion for RNA-seq data with DESeq2. *Genome Biol* **15**, 550 (2014).

27.   L. Kolberg, U. Raudvere, I. Kuzmin, J. Vilo, H. Peterson, gprofiler2 -- an R package for gene list functional enrichment analysis and namespace conversion toolset g:Profiler. *F1000Res* **9** (2020).

28.   U. Raudvere *et al.*, g:Profiler: a web server for functional enrichment analysis and conversions of gene lists (2019 update). *Nucleic Acids Res* **47**, W191-w198 (2019).

29.   D. Merico, R. Isserlin, O. Stueker, A. Emili, G. D. Bader, Enrichment map: a network-based method for gene-set enrichment visualization and interpretation. *PLoS One* **5**, e13984 (2010).

30.   M. Kucera, R. Isserlin, A. Arkhangorodsky, G. D. Bader, AutoAnnotate: A Cytoscape app for summarizing networks with semantic annotations. *F1000Res* **5**, 1717 (2016).

31.   L. Oesper, D. Merico, R. Isserlin, G. D. Bader, WordCloud: a Cytoscape plugin to create a visual semantic summary of networks. *Source Code Biol Med* **6**, 7 (2011).

32.   S.-K. Devan *et al.*, A MademoiseLLE domain binding platform links the key RNA transporter to endosomes. *PLOS Genet* **18**, e1010269 (2022).

33.   T. Langner *et al.*, Chitinases Are Essential for Cell Separation in *Ustilago maydis*. *Eukaryot Cell* **14**, 846-857 (2015).

34.   C. Haag, T. Klein, M. Feldbrügge, ESCRT Mutant Analysis and Imaging of ESCRT Components in the Model Fungus *Ustilago maydis*. *Methods Mol Biol* **1998**, 251-271 (2019).

35.   S. Baumann, T. Pohlmann, M. Jungbluth, A. Brachmann, M. Feldbrügge, Kinesin-3 and dynein mediate microtubule-dependent co-transport of mRNPs and endosomes. *J Cell Sci* **125**, 2740-2752 (2012).

36.   F. Madeira *et al.*, Search and sequence analysis tools services from EMBL-EBI in 2022. *Nucleic Acids Res* 10.1093/nar/gkac240, gkac240 (2022).

37.   K. Heimel *et al.*, The transcription factor Rbf1 is the master regulator for b-mating type controlled pathogenic development in *Ustilago maydis*. *PLoS Pathog* **6**, e1001035 (2010).

38.   D. Lanver *et al.*, The Biotrophic Development of *Ustilago maydis* Studied by RNA-Seq Analysis. *Plant Cell* **30**, 300-323 (2018).

39.   E. Vollmeister *et al.*, Tandem KH domains of Khd4 recognize AUACCC and are essential for regulation of morphology as well as pathogenicity in *Ustilago maydis*. *Rna* **15**, 2206-2218 (2009).

40.   C. Haag, T. Pohlmann, M. Feldbrügge, The ESCRT regulator Did2 maintains the balance between long-distance endosomal transport and endocytic trafficking. *PLoS Genet* **13**, e1006734 (2017).

41.   P. Becht, J. König, M. Feldbrügge, The RNA-binding protein Rrm4 is essential for polarity in *Ustilago maydis* and shuttles along microtubules. *J Cell Sci* **119**, 4964-4973 (2006).